A national laboratory of the U.S. Department of Energy
Office of Energy Efficiency & Renewable Energy

National Renewable Energy Laboratory

Innovation for Our Energy Future

# Study and Development of Anti-Islanding Control for Synchronous Machine-Based Distributed Generators

## November 2001 — March 2004

Z. Ye
*GE Global Research Center*
*Niskayuna, New York*

*Subcontract Report*
**NREL/SR-560-38018**
**March 2006**

NREL is operated by Midwest Research Institute • Battelle  Contract No. DE-AC36-99-GO10337

# Study and Development of Anti-Islanding Control for Synchronous Machine-Based Distributed Generators

## November 2001 — March 2004

Z. Ye
*GE Global Research Center*
*Niskayuna, New York*

NREL Technical Monitor: B. Kroposki

Prepared under Subcontract No. NAD-1-30605-01

***Subcontract Report***
**NREL/SR-560-38018**
**March 2006**

**National Renewable Energy Laboratory**
**1617 Cole Boulevard, Golden, Colorado 80401-3393**
**303-275-3000 • www.nrel.gov**

Operated for the U.S. Department of Energy
Office of Energy Efficiency and Renewable Energy
by Midwest Research Institute • Battelle

Contract No. DE-AC36-99-GO10337

**NOTICE**

This report was prepared as an account of work sponsored by an agency of the United States government. Neither the United States government nor any agency thereof, nor any of their employees, makes any warranty, express or implied, or assumes any legal liability or responsibility for the accuracy, completeness, or usefulness of any information, apparatus, product, or process disclosed, or represents that its use would not infringe privately owned rights. Reference herein to any specific commercial product, process, or service by trade name, trademark, manufacturer, or otherwise does not necessarily constitute or imply its endorsement, recommendation, or favoring by the United States government or any agency thereof. The views and opinions of authors expressed herein do not necessarily state or reflect those of the United States government or any agency thereof.

Available electronically at http://www.osti.gov/bridge

Available for a processing fee to U.S. Department of Energy
and its contractors, in paper, from:
U.S. Department of Energy
Office of Scientific and Technical Information
P.O. Box 62
Oak Ridge, TN 37831-0062
phone: 865.576.8401
fax: 865.576.5728
email: mailto:reports@adonis.osti.gov

Available for sale to the public, in paper, from:
U.S. Department of Commerce
National Technical Information Service
5285 Port Royal Road
Springfield, VA 22161
phone: 800.553.6847
fax: 703.605.6900
email: orders@ntis.fedworld.gov
online ordering: http://www.ntis.gov/ordering.htm

**This publication received minimal editorial review at NREL**

Printed on paper containing at least 50% wastepaper, including 20% postconsumer waste

# Table of Contents

**EXECUTIVE SUMMARY** ..... **1**

**1 INTRODUCTION** ..... **3**

**2 SYNCHRONOUS MACHINE AND POWER SYSTEM MODELING** ..... **5**

2.1 SYNCHRONOUS GENERATOR MODEL FOR ISLANDING STUDIES ..... 6

2.2 EXCITATION SYSTEM MODEL AND REACTIVE POWER REGULATION ..... 8

2.3 GOVERNOR MODEL AND ACTIVE POWER REGULATION ..... 9

2.4 RLC LOAD MODEL AND INDUCTION MOTOR LOAD MODEL ..... 10

2.5 GRID MODEL ..... 13

2.6 SMALL-SIGNAL ANALYSIS ..... 13

**3 ANTI-ISLANDING CONCEPT AND IMPLEMENTATION** ..... **15**

3.1 INTRODUCTION OF POSITIVE FEEDBACK ..... 15

3.2 IMPLEMENTATION OF THE ACTIVE/REACTIVE POWER SCHEMES ..... 15

3.3 DESIGN GUIDELINE BASED ON FREQUENCY-DOMAIN ANALYSIS ..... 17

3.4 PRACTICAL DESIGN CONSIDERATIONS ..... 19

*3.4.1 Power Level* ..... *19*

*3.4.2 Quality Factor* ..... *21*

*3.4.3 Grid Impedance* ..... *22*

*3.4.4 Motor Load* ..... *22*

*3.4.5 Conclusions* ..... *23*

**4 PERFORMANCE EVALUATION WITH TIME-DOMAIN SIMULATIONS** ..... **24**

4.1 PERFORMANCE EVALUATION WITH RLC LOAD ..... 24

*4.1.1 Case 1: Baseline without AI Scheme* ..... *24*

*4.1.2 Case 2: Active Power Scheme with $Q_f$=1.8* ..... *24*

*4.1.3 Case 3: Reactive Power Scheme with $Q_f$=1.8* ..... *25*

*4.1.4 Case 4: Active Power Scheme with $Q_f$=0.0* ..... *25*

*4.1.5 Case 5: Reactive Power Scheme with $Q_f$=0.0* ..... *25*

4.2 PERFORMANCE EVALUATION WITH INDUCTION MOTOR LOAD ..... 27

*4.2.1 Case 6: Baseline without AI Scheme and with Induction Motor Load* ..... *27*

*4.2.2 Case 7: Active Power AI Scheme with Induction Motor Load* ..... *27*

*4.2.3 Case 8: Reactive Power AI Scheme with Induction Motor Load* ..... *27*

4.3 PERFORMANCE EVALUATION WHEN THE GRID IS CONNECTED ..... 29

*4.3.1 Grid Disturbances* ..... *29*

*4.3.2 Grid Impedances* ..... *30*
*4.3.3 Grid Frequency Oscillations* ..... *32*
**5 SUMMARY** ..... **33**
5.1 CONCLUSIONS ..... 33
5.2 FUTURE WORK ..... 34
**6 APPENDIX** ..... **35**
6.1 SYNCHRONOUS MACHINE DATA ..... 35
6.2 INDUCTION MOTOR DATA ..... 36
**7 REFERENCES** ..... **37**

# List of Figures

Figure 1: Synchronous generator system and its control block diagram ..... 5
Figure 2: Synchronous generator d- and q-axis equivalent circuits ..... 8
Figure 3: Control block diagram of excitation system ..... 9
Figure 4: Control block diagram of governor ..... 10
Figure 5: DQ equivalent circuit model of RLC load ..... 11
Figure 6: DQ equivalent circuit model of induction motor ..... 12
Figure 7: DQ equivalent circuit model of grid ..... 13
Figure 8: DQ equivalent circuit model of the overall system ..... 14
Figure 9: Schematic of the machine with the AI compensators ..... 16
Figure 10: Schematic of the machine with the AI loops opened ..... 17
Figure 11: Active and reactive AI compensators ..... 18
Figure 12: Loop gains with different generator output power ..... 20
Figure 13: Loop gains with different quality factors ..... 21
Figure 14: Loop gains with different grid impedance ..... 22
Figure 15: Loop gains with RLC and motor load ..... 23
Figure 16: Simulation results of the active power scheme in response to islanding at 1s ..... 25
Figure 17: Simulation results of the reactive power scheme in response to islanding at 1s ..... 26
Figure 18: Simulation results with the induction motor load in response to islanding at 1s ..... 28
Figure 19: Simulation results of the generator response to a three-phase fault ..... 30
Figure 20: Simulation results with high grid impedance ..... 31
Figure 21: Simulation results of the generator response to the grid frequency oscillation ..... 32

# List of Symbols

$i_d$ , $i_q$ Direct-axis and quadrature-axis currents of the generator;

$u_d$ , $u_q$ Direct-axis and quadrature-axis voltage of the generator;

$i_{fd}$ Field winding current of the generator;

$e_{fd}$ Field voltage applied to the generator;

$i_{1d}$ , $i_{1q}$ Direct-axis and quadrature-axis damper winding currents of the generator;

$R_a$ Stator winding resistance of the generator;

$R_{fd}$ Field winding resistance of the generator;

$R_{1d}$ , $R_{1q}$ Damper winding resistance of the generator;

$L_l$ Stator winding inductance of the generator;

$L_{fd}$ Field winding leakage inductance of the generator;

$L_{1d}$ , $L_{1q}$ Direct and quadrature damper winding inductance of the generator;

$L_{ad}$ , $L_{aq}$ Direct and quadrature magnetizing inductances of the generator;

$\omega_r$ Rotating speed of the generator;

$\delta$ Power angle of the generator;

$T_m$ Mechanical torque of the generator;

$T_e$ Electromagnetic torque of the generator;

$H$ Inertia constant of the generator;

$\Psi_d$ , $\Psi_q$ Direct and quadrature flux linkage of the generator;

$\Psi_{fd}$ Field flux linkage of the generator;

$\Psi_{1d}$ , $\Psi_{1q}$ Direct and quadrature damper windings flux linkage of the generator;

$V_A$ , $V_B$ State variables of the exciter;

$K_1$ , $K_2$ , $K_3$ Constant gain of the excitation system controller;

$T_1$ , $T_2$ , $T_3$ Time constant of the excitation system controller;

$P_{ref}$ , $Q_{ref}$ Reference value for the active and reactive power;

$Q_e$ Reactive power output of the generator;

$V_{ref}$ Reference of the generator terminal voltage;

| | |
|---|---|
| $V_t$ | Terminal voltage of the generator; |
| $T_G$ | Time constant of the prime mover of the generator; |
| $R_G$ | The governor droop constant; |
| $i_{dR}$ , $i_{qR}$ | D-axis and q-axis currents of the resistance load; |
| $i_{dL}$ , $i_{qL}$ | D-axis and q-axis currents of the inductance load; |
| $i_{dC}$ , $i_{qC}$ | D-axis and q-axis currents of the capacitance load; |
| $R$ , $L$ , $C$ | Load resistance, capacitance and inductance; |
| $e_{dm}$ , $e_{qm}$ | D-axis and q-axis components of the induction motor transient stator voltage; |
| $i_{dm}$ , $i_{qm}$ | D-axis and q-axis components of induction motor transient stator current; |
| $X_{sm}$ | Synchronous inductance of the induction motor; |
| $X'_{sm}$ | Transient inductance of the induction motor; |
| $H_m$ | Inertia constant of the induction motor; |
| $D$ | Load model exponent of the motor; |
| $T_{norm}$ | Normal value of mechanical torque of the motor; |
| $R_e$ , $L_e$ | Grid resistance and inductance; |
| $V^{\infty}$ | Rms value of the infinite bus voltage; |
| $\alpha$ | Phase angle of the infinite bus; |
| $i_{dgrid}$ , $i_{qgrid}$ | D-axis and q-axis currents flowing into the grid; |
| $G_{pai}$ , $G_{qai}$ | Active power and reactive power AI compensator transfer functions. |

# List of Acronyms

| | |
|---|---|
| AI | Anti-islanding |
| AVR | Automatic voltage regulator |
| DG | Distributed generator |
| kW | Kilowatt |
| PI | Proportional - Integral |
| ROCOF | Rate of change of frequency relay |
| THD | Total Harmonic Distortion |

# Executive Summary

This report summarizes the study and development of new active anti-islanding (AI) control schemes for synchronous machine-based distributed generators (DGs). These DGs include engine generators (diesel, natural gas, biomass, hydrogen) and gas turbines.

The accomplishments of the work include:

1. Advancing new AI control schemes that exhibit substantial improvement on non-detection zone for a static load, without power quality degradation. The schemes also lower costs and feature robustness for system disturbances
2. Providing design guidelines and evaluating the effectiveness of the new schemes under various load conditions
3. Validating the new anti-islanding control schemes with a time-domain simulation in PSCAD.

The report presented here is divided into four parts. The first part discusses the modeling of basic system components, including the synchronous machine, and the RLC and induction motor loads, and the grid. The second part of the report discusses in detail the basic principles and design guidelines of the new AI schemes, denoted as active power AI scheme and reactive power AI scheme respectively. Frequency-domain results in MATLAB are used for the analysis. In the third part, time domain simulations are carried out using PSCAD to validate the effectiveness of the proposed schemes. Finally, conclusions based on the theoretical analysis and the simulation results are provided. The future scope of work along with issues to be addressed is also established.

# 1. Introduction

The phenomenon of islanding in the presence of distributed generation systems (DGs) requires considerable attention due to its potential result in an unsafe operating condition of the system. Almost all utilities require that, in case of islanding, generators should disconnect from the grid as soon as possible. IEEE standard 1547 stipulates a maximum delay of 2s for detection of an island and also establishes the need for proper coordination of the auto-reclosing scheme with the anti-islanding (AI) protection [1]. While the past decade has seen the introduction of many new concepts, several outstanding issues remain especially with regard to availability of reliable and economical AI schemes for rotating-machine-based distributed generators.

To prevent unintentional islanding, transfer trip is traditionally used, mostly for larger units in megawatt ranges. For smaller DGs connected at distribution level, transfer trip is too expensive. Also, an increasing number of distribution systems are configured to provide multiple alternate feed points to a particular feeder section. Transfer trip can be exceedingly complicated and expensive to implement when trip signals from multiple points need to be communicated, as well as the current status of the system configuration to determine which trip signal is relevant at any given time. While other low-cost communication means and infrastructures are under development, it is always desirable for DG to have local intelligence to detect islanding events.

The most basic and universal means of detecting an island is to establish an under/over frequency and under/over voltage window within which a synchronous DG is allowed to operate. When the synchronous DG is islanded from the utility system, either due to a fault or other abnormal condition, the frequency and voltage will quickly move outside the operating window if there is a significant difference between loads and the generation level. For generations that are not designed to export power to the utility network, the loss of the grid connection inherently causes power to flow from the generator into the utility network to supply other loads left connected to the islanded subsystem. This can be detected using a reverse power relay to monitor the power flow in the inter-tie, which can be used to trip the inter-tie breaker.

With large generators, there is a reasonable possibility that the system voltage and frequency will be maintained within the specified limits following loss of the grid. Therefore, special means are required to detect the loss of the grid. Depending whether there is interaction with the system or not, they can be divided into two categories: passive and active.

Active schemes detect the islanding by directly interacting with the system under consideration. The two main methods used for synchronous machines are reactive error export detection and fault level monitoring [3-4]. The reactive error export detector controls the embedded generator excitation current so that it generates a known value of reactive current, which cannot be supported unless the generator is connected to the grid. The fault level monitoring scheme uses point-on-wave thyristor switching, which triggers near the voltage zero point, and then measures the current through a shunt inductor, enabling calculation of system impedance and fault level. The fault level monitoring scheme provides a very fast response to the condition with detection possible in half a cycle.

Passive devices function by monitoring various system parameters and make their decision to trip without directly interacting with the system operation. Typical passive techniques include the rate of change of frequency relay (ROCOF) [5-6]; rate of change of output power [7-8]; ratio of the frequency change to the output power change [9]; rate of change of voltage and power factor [10]; detection of islanding using an elliptical trajectory technique [11]; voltage unbalance; and total harmonic distortion (THD) [12], etc. These technologies were developed based on the fact that a loss of the grid will cause variations in system

voltage, current, or frequency under almost all circumstances. Nevertheless, when the amount of power mismatch between utility and local load is not significant, it may fail to signal the abnormality.

The main drawback to the passive schemes is that they cannot effectively differentiate between the loss of the grid and other non-islanding transients. Active schemes are more effective and robust than the passive schemes, but most existing active schemes have the disadvantages of high cost and degradation of power quality. Therefore, it is imperative to find new means of protecting DG against islanding reliably and economically. Otherwise, as other technologies in the field of distributed resources are advancing, the lack of reliable protection against islanding is impeding the wide deployment of these alternative energy resources.

The objective of this study is to develop new effective AI schemes for synchronous machine-based distributed generators.

# 2. Synchronous Machine and Power System Modeling

Unintentional islanding is considered undesirable for a number of reasons including worker and public safety. The effective detection of islanding is a real issue confronting power system engineers. The worst-case islanding is when the power mismatch between the DG and the load is zero, and the system is operating at steady state before islanding. This is the case on which this study will focus.

Synchronous generators can be analyzed conveniently using the Park's transformation, which results in a time-invariant nonlinear system. A linearized model can be obtained from the time-invariant model at a steady-state operating point. In the event that the system experiences a small perturbation, the linearized power system models can be used with advantage for both analysis and controller design. Such a linear design on a nonlinear system generally provides asymptotic stability over a small region about the equilibrium and is appropriate for the dynamic stability problem where the primary concern is providing damping following small disturbances.

The mathematical model of a synchronous machine along with various control strategies has been well documented in the literature [13]. For completeness, the model of a machine used in the analysis is reported here again in detail. The overall control block diagram of machine model is shown in the Figure 1. The most noticeable feature here is that when the generator is connected to the grid, the main task of the generator is to maintain its real and reactive power output as a typical DG operational mode (in some cases, instead of reactive power, power factor regulation is used). The regulation of the real power is achieved through a feed-forward controller applied to the governor while the regulation of the reactive power is carried out through a feedback PI (Proportional-Integral) controller cascaded with the exciter.

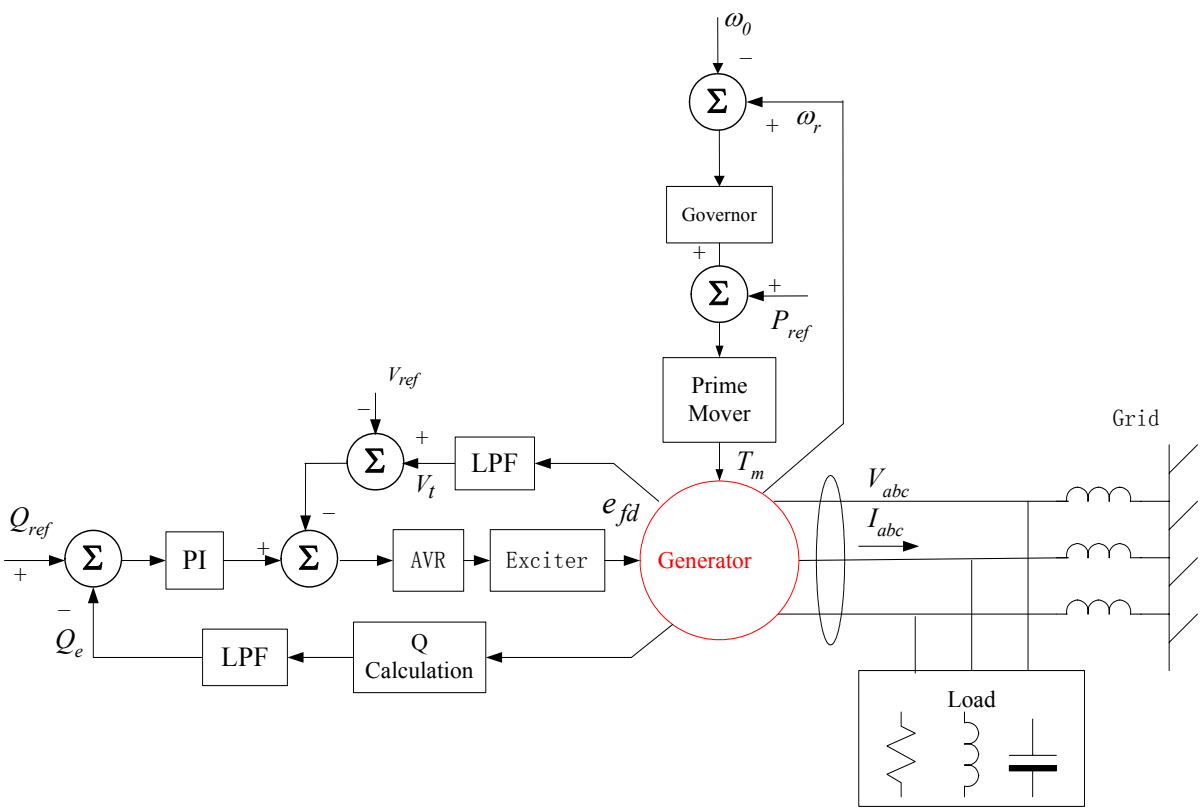


Figure 1: Synchronous generator system and its control block diagram

## 2.1 Synchronous Generator Model for Islanding Studies

The dynamics of the synchronous machine can be described by a set of nonlinear differential equations. Typically, the states can be associated with each machine's armature currents, rotor currents resolved through the Park's equations, rotor dynamics, automatic voltage regulator (AVR) and the turbine-governor dynamics.

In developing the model of a synchronous machine for islanding studies, the following assumptions were made. The worst-case islanding is when the power mismatch is small and the system is operating under steady-state conditions before islanding. This provides solid justification for the following assumptions:

1. The air gap flux is distributed sinusoidally along the air gap.
2. Magnetic hysteresis is negligible.
3. Magnetic saturation effects are neglected.

After simplifications, the following set of equations of the machine model can be obtained.

*Voltage equations*

$$u_d = p\Psi_d - \Psi_q \omega_r - R_a i_d \tag{2.1}$$

$$u_q = p\Psi_q + \Psi_d \omega_r - R_a i_q \tag{2.2}$$

$$e_{fd} = p\Psi_{fd} + R_{fd} i_{fd} \tag{2.3}$$

$$0 = p\Psi_{1d} + R_{1d} i_{1d} \tag{2.4}$$

$$0 = p\Psi_{1q} + R_{1q} i_{1q} \tag{2.5}$$

*Flux linkage equations*

$$\Psi_d = -(L_{ad} + L_l) i_d + L_{ad} i_{fd} + L_{ad} i_{1d} \tag{2.6}$$

$$\Psi_q = -(L_{aq} + L_l) i_q + L_{aq} i_{1q} \tag{2.7}$$

$$\Psi_{fd} = (L_{ad} + L_{fd}) i_{fd} + L_{ad} i_{1d} - L_{ad} i_d \tag{2.8}$$

$$\Psi_{1d} = L_{ad} i_{fd} + (L_{1d} + L_{ad} i_{fd}) i_{1d} - L_{ad} i_d \tag{2.9}$$

$$\Psi_{1q} = (L_{1q} + L_{aq}) i_{1q} - L_{aq} i_q \tag{2.10}$$

*Air-gap torque*

$$T_e = \Psi_d i_q - \Psi_q i_d \tag{2.11}$$

Here the flux is denoted by $\Psi$. Inductance is denoted by L, and terminal voltage is expressed in the D-Q frame [13]. Generally, in case of synchronous machines, the prime mover and other essential mechanical assemblies are mounted on the same shaft. Based on the time frame involved, it is fairly a good approximation to assume the rotor mass as a rigid body. Hence for the islanding studies, the following differential equations are used to represent the synchronous machine rotor dynamics.

$$\frac{d^2\delta}{dt} = \frac{1}{2\mathrm{H}}(T_m - T_e) \tag{2.12}$$

$$\frac{d\delta}{dt} = \omega_r - \omega_0 \tag{2.13}$$

where:

$i_d$ and $i_q$ are direct-axis and quadrature-axis currents of the generator;

$u_d$ and $u_q$ are direct-axis and quadrature-axis voltage of the generator;

$i_{fd}$ is field winding current of the generator;

$e_{fd}$ is field voltage applied to the generator;

$i_{1d}$ and $i_{1q}$ are direct-axis and quadrature-axis damper winding currents of the generator;

$R_a$ is stator winding resistance of the generator;

$R_{fd}$ is field resistance of the generator;

$R_{1d}$ and $R_{1q}$ are damper winding resistance of the generator;

$L_l$ is stator winding inductance of the generator;

$L_{fd}$ is field leakage inductance of the generator;

$L_{1d}$ and, $L_{1q}$ are direct and quadrature leakage inductance of the generator;

$L_{ad}$ and $L_{aq}$ are direct and quadrature magnetizing inductance of the generator;

$\omega_r$ is rotating speed of the generator;

$\delta$ is power angle of the generator;

$T_m$ is mechanical torque of the generator;

$T_e$ is electromagnetic torque of the generator;

$H$ is inertia constant of the generator;

$\Psi_d$ and $\Psi_q$ are direct and quadrature flux linkage of the generator;

$\Psi_{fd}$ is field winding flux linkage of the generator;

$\Psi_{1d}$ and $\Psi_{1q}$ are direct and quadrature damper winding flux linkage of the generator.

Based on equations (2.1)–(2.13), an equivalent circuit of the synchronous machine can be developed as shown in the Figure 2.

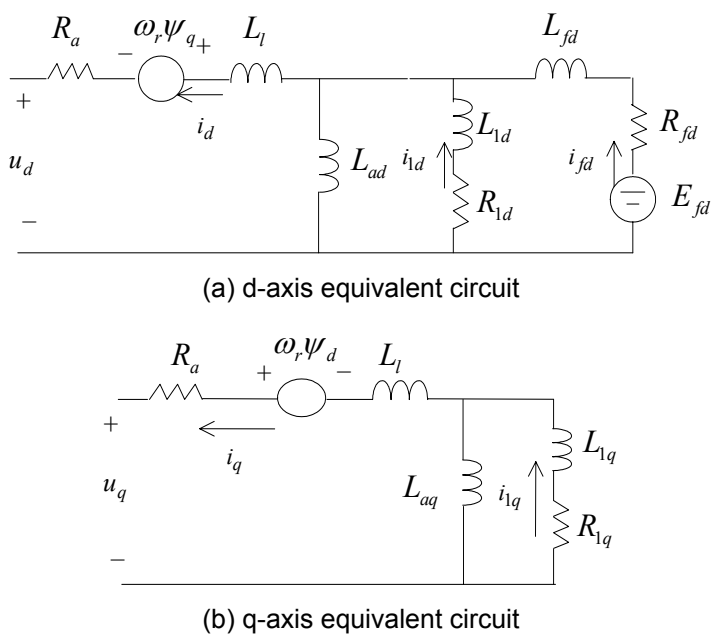


Figure 2: Synchronous generator d- and q-axis equivalent circuits

## *2.2 Excitation System Model and Reactive Power Regulation*

Most generators are equipped with an AVR. These devices maintain the terminal voltage of the generator at a specified value by modulating the field voltage and hence the field current to supply the required reactive power to the load. However, as a distributed generation, the voltage regulation is prohibited by IEEE 1547, unless special agreements are made. A common operation mode for DG is reactive power (or power factor) regulation.

The exciter systems widely used for synchronous machines are commonly subdivided into the four different categories. More detailed aspects of modeling an excitation system for simulation studies can be found in [14]. For simplicity of analysis in the time frame involved, the excitation system here is represented as a tuned PI controller with a necessary lag circuit. The parameters of the circuit model are approximated from the aggregate response of terminal voltage of a generator. Figure 3 shows the model of the excitation system used for the machine simulation. A feedback PI controller is cascaded with the exciter to regulate the reactive power of the machine. Therefore, when the grid is connected, the reactive power output of the machine will follow the desired reference value. The parameters of the PI controller are given in the Appendix of this report.

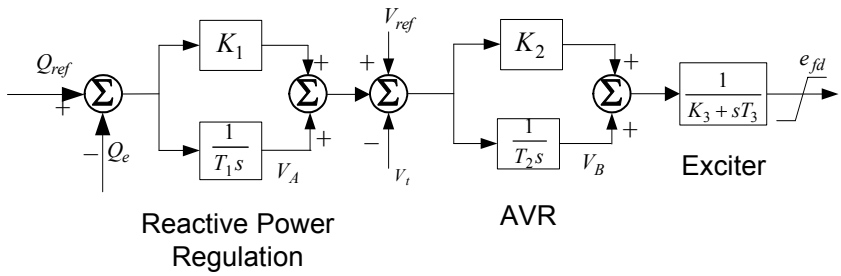


Figure 3: Control block diagram of excitation system

The description of the reactive power regulator and the exciter is given by:

$$\dot{V}_A = (Q_{ref} - Q_e)/T_1 \tag{2.14}$$

$$\dot{V}_B = [V_{ref} - V_t + V_A + K_1(Q_{ref} - Q_e)]/T_2 \tag{2.15}$$

$$\dot{e}_{fd} = [V_B - K_3 e_{fd} + K_2(V_{ref} - V_t + V_A + K_1(Q_{ref} - Q_e))]/T_3 \tag{2.16}$$

where:

$V_A$ and $V_B$ are the intermediate variables indicated in Figure 3;

$K_1, K_2$ and $K_3$ are constant in the controller;

$T_1, T_2$ and $T_3$ are time constant in the controller;

$Q_{ref}$ is the reference value of the reactive power;

$Q_e$ is the reactive power output of the generator;

$V_{ref}$ is the reference for the terminal voltage;

$V_t$ is the terminal voltage of the generator;

$e_{fd}$ is the field voltage as the input to the generator.

## 2.3 Governor Model and Active Power Regulation

The governor system consists of a prime mover and provides the necessary mechanical power required by the generator. The governor is represented by a droop function with $P_{ref}$ input and the prime mover is described by a lag function. Figure 4 shows the typical representation of a governor and the real power regulation for these islanding studies:

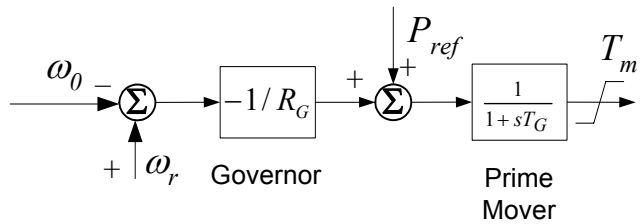


Figure 4: Control block diagram of governor

The governor dynamics is (including the prime mover)

$$\dot{T}_m = \frac{1}{T_G}(P_{ref} + \frac{\omega_0 - \omega_r}{R_G} - T_m) \tag{2.17}$$

where:

$T_G$ is the time constant of the prime mover of the generator;

$R_G$ is the governor droop.

## 2.4 RLC Load Model and Induction Motor Load Model

Load characteristics have an important influence on the dynamical behavior of the generator when it is islanded. The modeling of actual loads is complicated because a typical load bus is composed of a large number of devices, such as fluorescent and incandescent lamps, refrigerators, heaters, compressors, motors, furnaces, and so on. Based on a considerable amount of simplification, two types of the loads are most often investigated in the islanding studies: a RLC load and an induction motor load.

The RLC load is as simple as the aggregation of a resistor—an inductor and a capacitor in parallel. While such a load can represent the steady-state fundamental frequency characteristics of an actual load, this type of model is not a realistic representation of a load because the dynamic and non-fundamental characteristics of actual loads are not accurately simulated. Given the terminal voltage, the current through the resistance, inductance and the capacitance is determined by the following equations.

$$\frac{d}{dt}\begin{pmatrix} i_{dL} \\ i_{qL} \end{pmatrix} = \frac{1}{L}\begin{pmatrix} u_d \\ u_q \end{pmatrix} + \omega\begin{pmatrix} i_{qL} \\ -i_{dL} \end{pmatrix} \tag{2.18}$$

$$\frac{d}{dt}\begin{pmatrix} u_{dC} \\ u_{qC} \end{pmatrix} = \omega\begin{pmatrix} u_q \\ -u_d \end{pmatrix} + \frac{1}{C}\begin{pmatrix} i_{dc} \\ i_{qc} \end{pmatrix} \tag{2.19}$$

$$\begin{pmatrix} i_{dR} \\ i_{qR} \end{pmatrix} = 1/R\begin{pmatrix} u_d \\ u_q \end{pmatrix} \tag{2.20}$$

where:

$i_{dR}$ $i_{qR}$, $i_{dL}$ $i_{qL}$ and $i_{dC}$ $i_{qC}$ are the d-axis and q-axis currents through the load resistance, inductance and capacitance, respectively

$u_d$ $u_q$ are d-axis and q-axis terminal voltage

$R$, $L$, and $C$ are the value of load resistance, capacitance and inductance, respectively.

The RLC load equivalent circuit in DQ is shown in Figure 5.

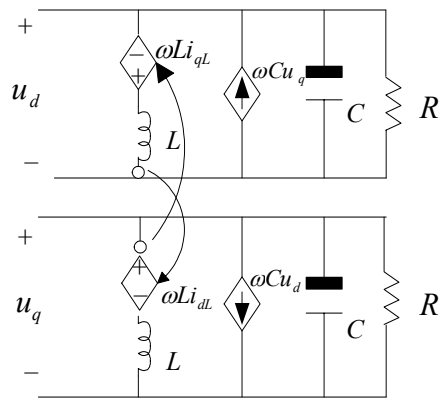


Figure 5: DQ equivalent circuit model of RLC load

Typically, motors consume 20% to 70% of the total energy supplied by a feeder. Therefore, the dynamics attributable to motors are usually the most significant aspects of dynamic characteristics of the overall system load. Motor loads, however, vary largely in characteristics due to different applications. The motor load used in the simulation studies described in this report is a compromise; it is intended to represent a general population of motors ranging in types from those in small residential/industrial applications to large motors. The default motor load uses only a single-cage representation. This is adequate for dynamic stability studies where damping of oscillations, rather than stalling of motors and motor starting, is the main focus.

The induction motor to be studied is represented by a standard single-cage model with the transient variations of its rotor flux linkage handled explicitly. The motor can be described by performance-based parameters or equivalent circuit parameters. The driven load is characterized by the inertia constant $H_m$ of the combined motor-load rotor and the exponent D, relating driven load to its speed. The detailed modeling of the motor load can be found in reference [15]. The dynamics of the induction motor is described by

$$\dot{e}_{dm} = -\frac{1}{T_0^{'}}(e_{dm} + (X_{sm} - X_{sm}^{'})i_{qm}) + p\theta_r e_{qm} \tag{2.21}$$

$$\dot{e}_{qm} = -\frac{1}{T_0^{'}}(e_{qm} - (X_{sm} - X_{sm}^{'})i_{dm}) - p\theta_r e_{dm} \tag{2.22}$$

$$2H_m\dot{\omega}_m = (e_{qm}i_{qm} + e_{dm}i_{dm}) - T_{norm}(\frac{\omega_m}{\omega_0})^D \tag{2.23}$$

where:

$e_{dm}$, $e_{qm}$ are D-axis and q-axis components of the motor transient stator voltage;

$i_{dm}$, $i_{qm}$ are D-axis and q-axis components of the motor transient stator current;

$X_{sm}$ is the motor synchronous inductance;

$X_{sm}^{'}$ is the motor transient inductance;

$H_m$ is inertia constant of the motor;

$D$ is load model exponent of the motor;

$T_{norm}$ is normal value of mechanical torque of the motor;

$\omega_m$ is rotating speed of the motor.

Figure 6 shows the DQ equivalent circuit of the induction motor.

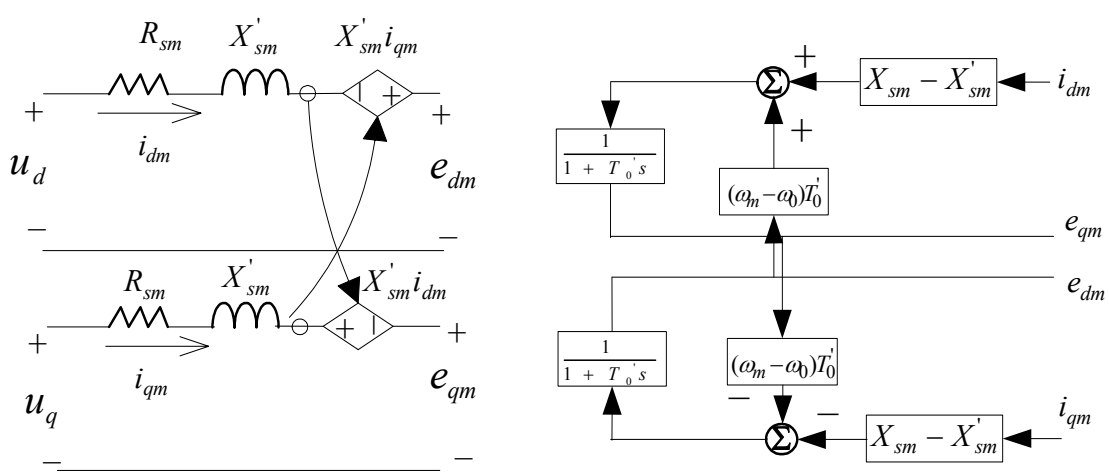


Figure 6: DQ equivalent circuit model of induction motor

## 2.5 Grid Model

Since the synchronous machine is connected to an infinite bus, the d-q terminal voltage of the machine are constrained by the grid voltage, described in DQ frame below:

$$\begin{pmatrix} u_d \\ u_q \end{pmatrix} = R_e \begin{pmatrix} i_{dgrid} \\ i_{qgrid} \end{pmatrix} + L_e \begin{pmatrix} \dot{i}_{dgrid} \\ \dot{i}_{qgrid} \end{pmatrix} - \omega L_e \begin{pmatrix} i_{qgrid} \\ -i_{dgrid} \end{pmatrix} + V^{\infty} \begin{pmatrix} \sin(\delta + \alpha) \\ \cos(\delta + \alpha) \end{pmatrix} \quad (2.24)$$

where:

$R_e$ and $L_e$ are the grid resistance and inductance respectively;

$V^{\infty}$ is the rms value of the bus voltage and $\alpha$ is its phase angle;

$i_{dgrid}$ and $i_{qgrid}$ are the d-axis and q-axis currents flowing into the grid.

Figure 7 shows the grid DQ equivalent circuit.

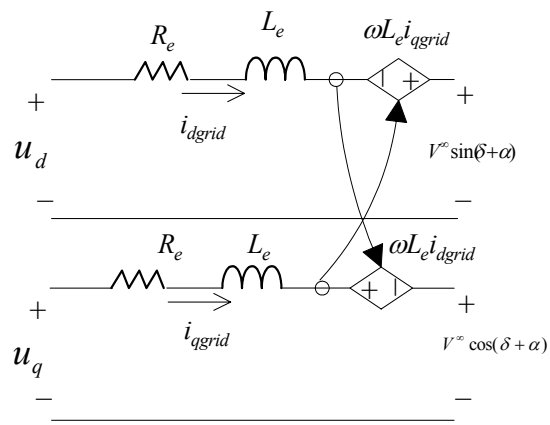


Figure 7: DQ equivalent circuit model of grid

## 2.6 Small-Signal Analysis

In the preceding section, we have developed the equivalent DQ circuit model for the generator, load and the grid respectively. The equivalent circuit of the overall system to be studied can be easily obtained by combining those components together. One circuit model of such a system consisting of the DG and the RLC load, and the grid is shown in Figure 8. This equivalent circuit is highly nonlinear and cross-coupled. If the perturbation applied to the power system is small, the linearized model, also called small-signal model, can be obtained by linearizing the equations from (2.1) to (2.24) around an operation point. Therefore, the highly nonlinear model can be greatly simplified and the dynamical characteristics of the power system can be approximately analyzed from the small-signal model.

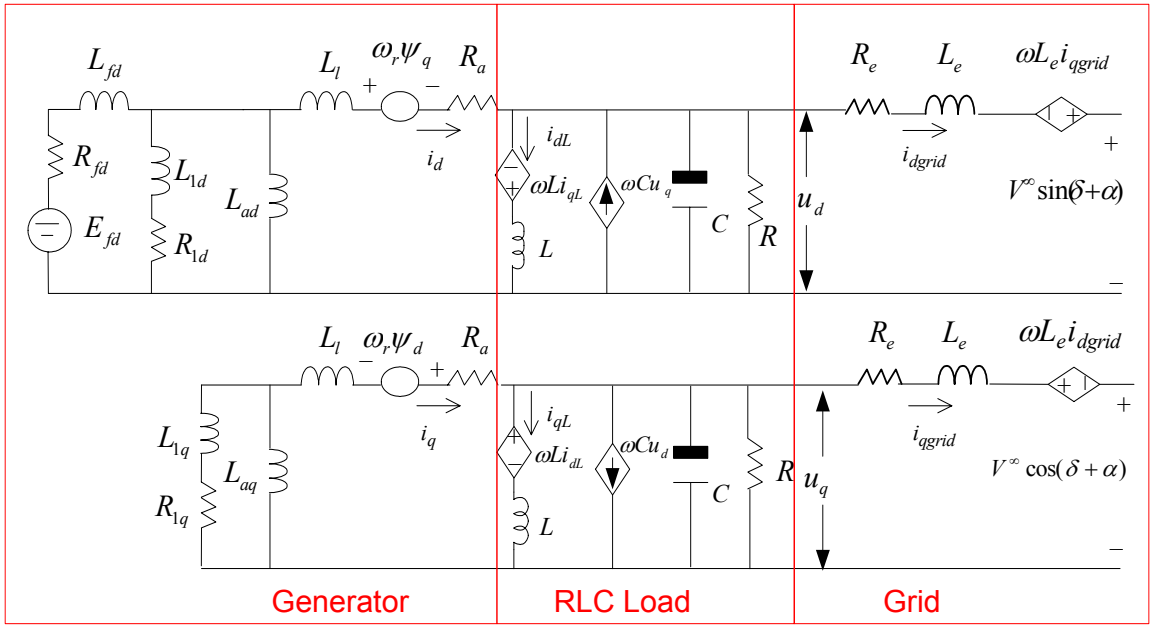


Figure 8: DQ equivalent circuit model of the overall system

# 3. Anti-Islanding Concept and Implementation

## *3.1 Introduction of Positive Feedback*

The proposed AI schemes for the synchronous machine DG are implemented on the basis of a positive feedback. The principle behind the method is to destabilize frequency or voltage by introducing positive feedback. This results in under/over frequency or voltage trip vary quickly once the DG is islanded. In the presence of the grid, the positive feedback will have little effect on the grid frequency or voltage regulation. In contrast to the passive methods, these active schemes can detect islanding effectively and reliably without causing false trip.

Although the positive feedback concept has been successfully used for the inverter-based DG for AI protection, the application of the concept to synchronous machine has not yet been explored extensively. Typically, a rotating-machine-based DG is characterized by higher inertia—longer time constants than an inverter-based DG. Due to these factors, the machine and the inverter-based DG respond in fundamentally different ways.

In support of the design and implementation, both frequency-domain and the time-domain analysis are conducted to provide the insights into the characteristics of the proposed schemes.

## *3.2 Implementation of the Active/Reactive Power Schemes*

The positive feedback for the synchronous machine comes in two different ways, denoted as active power AI scheme and reactive power AI scheme, because the feedback modifies the active power and reactive power references, respectively. The structures of the active and reactive power AI scheme are shown in Fig. 3-1. The active power AI compensator takes the variations in the frequency as input to modify the active power reference to the DG. The reactive power AI compensator uses the variation in the voltage magnitude to change the reactive power reference.

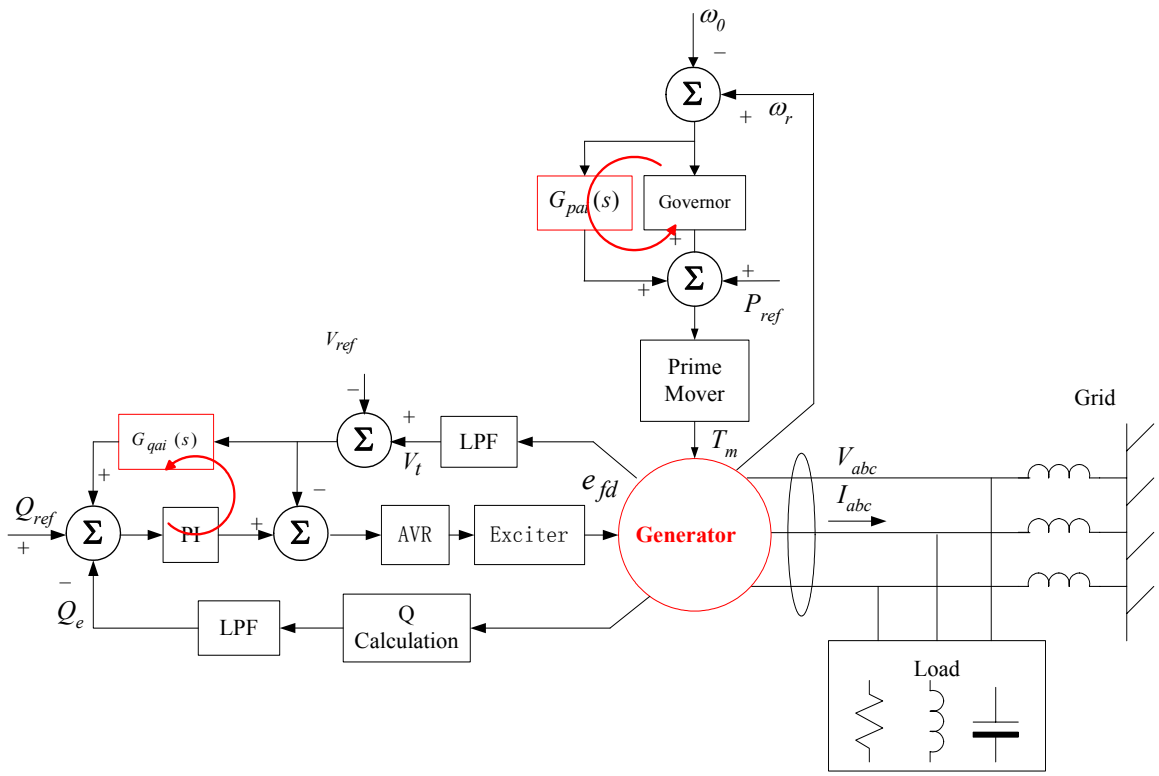


Figure 9: Schematic of the machine with the AI compensators

The AI compensators both consist of a washout filter and a proportional gain. The washout filter is designed to ensure that the AI compensators only react to the transient of the frequency/voltage, but not causing any DC steady-state error. When there is a voltage or frequency variation, the responses of the AI loop will amplify the voltage or frequency variation in the same direction. Therefore, the loops are called positive feedback. The mechanism can be further illustrated below.

When there is a generator terminal voltage variation, for instance, voltage increases slightly, and the reactive power reference will be increased due to the reactive power AI loop, which will lead to a boosted voltage reference, thus causing the terminal voltage to further increase. When properly designed, the effect of the reactive power AI loop is insignificant when the grid is connected because the grid will regulate the terminal voltage magnitude. Once grid is lost, the reactive power AI loop becomes dominant and drives the voltage away from nominal.

A similar mechanism applies to the frequency. When there is a generator speed (frequency) variation, e.g., when frequency increases slightly (due to under loading), the active power reference will be increased due to the active power AI loop, which will further generate a greater mechanical torque (resulting in more under loaded), causing higher speed (frequency). When properly designed, the mechanism will create this instability only in an islanded system and cause a frequency relay to trip.

In summary, the main idea is that the active/reactive power AI compensators have a dominant effect in the frequency/voltage oscillations when the grid connection is lost. But, with a proper design, these destabilization effects are negligible, when the machine is connected to the grid.

## 3.3 Design Guideline Based on Frequency-Domain Analysis

The basic principles of the positive feedback for islanding detection have been introduced. This section will emphasize on the design and implementation of the AI compensator. In order to illustrate the design guideline, a loop gain concept is used. MATLAB is used for the following frequency-domain analysis.

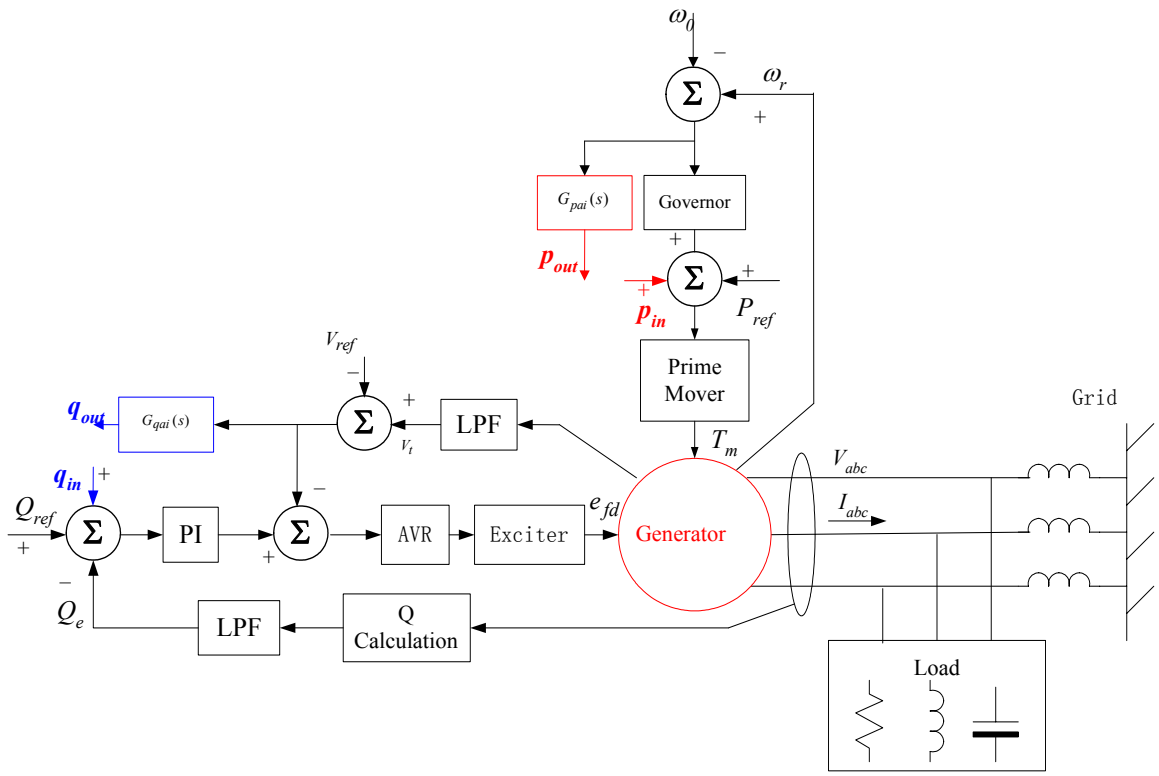


Figure 10: Schematic of the machine with the AI loops opened

The loop gains of the active and reactive AI loops can be measured by breaking the loops, shown in Figure 10, where $p_{in}$ and $p_{out}$ are at the breaking point for the active power loop, while $q_{in}$ and $q_{out}$ are for the reactive power loop. The loop gain is defined as the small-signal transfer function from the perturbation signal $p_{in}$ (or $q_{in}$) to the output $p_{out}$ (or $q_{out}$). Therefore, the active power loop gain is given by:

$$T_p(s) = \frac{p_{out}}{p_{in}} \tag{3.5}$$

Similarly, the reactive power AI loop gain is defined as the small signal transfer function from the perturbation signal from $q_{in}$ to the output $q_{out}$.

$$T_q(s) = \frac{q_{out}}{q_{in}} \tag{3.6}$$

From the loop gain, the system dynamics can be characterized by, for example, the stability margins. For AI control, the design principles are:

(1) When the grid is connected, the loop gain should indicate a stable system, i.e., the peak of the AI loop gain must be less than 0dB. The lower the loop gain is below 0dB, the less impact of the AI loop on the DG's normal grid-connected operation.

(2) When the grid is disconnected, the loop gain should indicate an unstable system, i.e., the peak of the AI loop gain must be greater than 0dB, while the phase is lagging more than 180 degrees. The unstable system will ensure that the islanded system can be detected even when there is 100% active and reactive power matching. The higher the loop gain, the more quickly the island voltage or frequency will move outside the normal operational windows to trigger voltage or frequency protection. However, on the other hand, the gain should not be too high to insure that criterion (1) is met. Basically, criterion (1) sets the upper bound of the loop gain, while criterion (2) sets the lower bound of the loop gain.

If both criteria are satisfied, the AI compensator will amplify the frequency/voltage transients when the machine is islanded but with minimal effect on the frequency/voltage dynamics when the grid is connected.

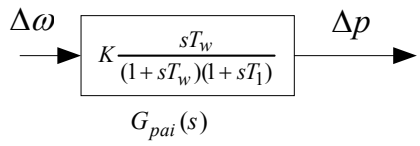


(a) Active power AI compensator

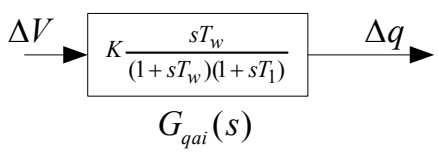


(b) Reactive power AI compensator

Figure 11: Active and reactive AI compensators

Figure 11 shows the formula of the active/reactive power AI compensator. The AI compensator basically consists of a washout filter, a gain and a first-order filter. The crucial step in the design is to determine the setting for the active/reactive power AI compensator. The critical settings include:

(1) The corner frequency of the washout filter, $T_W$

(2) The gain, K

(3) The low pass filter conner frequency $T_1$.

The washout function serves as a high-pass filter, with a time constant $T_W$ to allow signals with frequency higher than $1/T_W$ to pass. For the signal with frequency lower than $1/T_W$, especially for DC signal, will be attenuated by the washout filter. This is to minimize the AI loop impact on the steady-state regulation. The low pass filter corner frequency T1 is set to attenuate high-frequency noise. The combined washout filter and the low-pass filter constitute a band-pass filter. The selection of gain, K is a compromise between the high enough gain to ensure islanding detection quickly and the low enough gain to have minimal impact on the DG under the grid-connected conditions. The gain selection should leave certain margins for both grid-connected and islanded conditions.

## *3.4 Practical Design Considerations*

The basic criteria for the AI design have been discussed. However, the parametric design of the AI compensator is still an issue since the active/reactive power loop gains may vary with the different load conditions. In order to ensure that the AI control is effective under all circumstances, the AI compensator must be designed under the worst-case situation. The critical gain can only be approximately determined after the study of a range of different load conditions. Consequently, the impact of the various passive and motor load conditions on the loop gains must also be examined. The preliminary study concludes that the situations important to this AI scheme design are those where the grid impedance is high or there is a high penetration of induction motor load.

After the worst cases have been identified, the active and reactive power AI compensators are chosen as in (3.7) and (3.8), respectively.

$$\frac{\Delta p}{\Delta \omega} = \frac{61.1s}{(1+0.32s)(1+0.29s)} \tag{3.7}$$

$$\frac{\Delta q}{\Delta V} = \frac{2.41s}{(1+0.048s)(1+0.016s)} \tag{3.8}$$

When the analysis of the loop gains are carried out in the following, it is assumed that

1. The power output of the machine and the local load are closely matched.
2. The machine operates at a power factor of 1.0 (due to the choice of the RLC load with unity power factor).
3. The loss of the grid is caused by the tripping of the utility breaker at a moment when the system is operating at steady state.

With these assumptions, the impact of four different factors (power level, load quality factor, motor load and grid impedance) on the proposed AI schemes is investigated.

### 3.4.1 Power Level

In order to examine the impact of the different power level on the loop gain, the generator active power, which matches the active power of the RLC load (with $Q_f$ =1.8), is varied from 30% to 90%. The Bode plots of the loop gains under different power levels are shown in Figure 12.

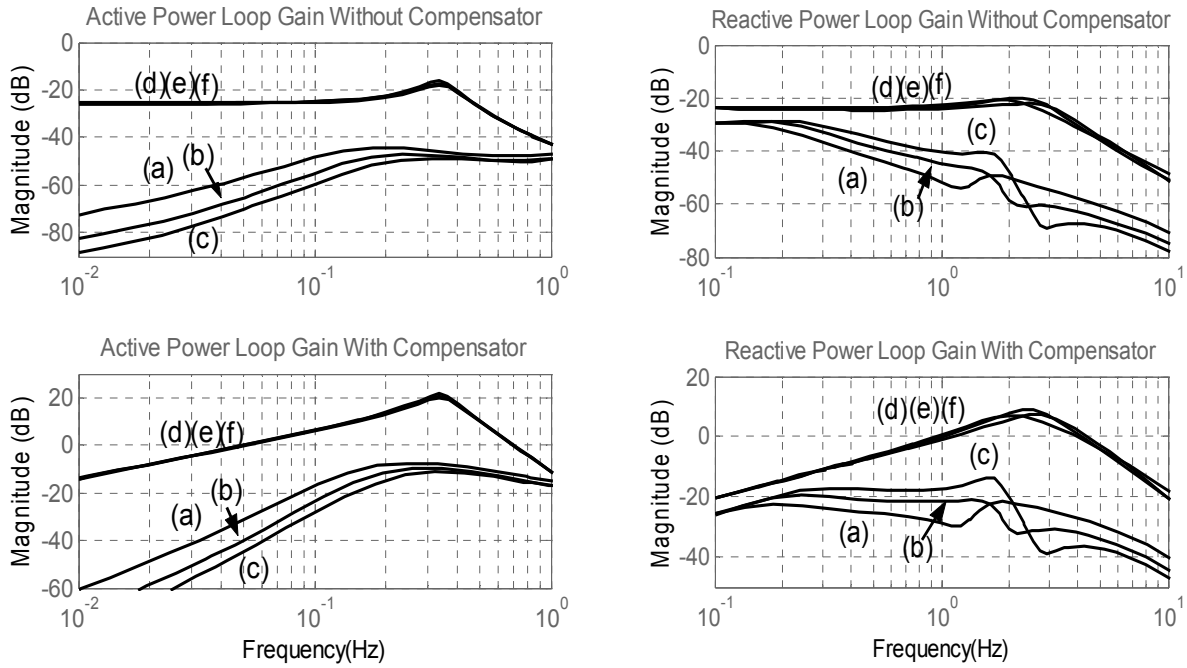


(i) Active power loop gains (ii) Reactive power loop gains

[(a) (b) (c) Grid-connected 30% power; 60% power; 90% power, (d) (e) (f) Grid-disconnected 30% power; 60% power; 90% power]

Figure 12: Loop gains with different generator output power

Without any compensator, both the active power and reactive power loop gains are much less than 0dB, under both grid connected [cases (a)(b)(c)] and islanded conditions [cases (d)(e)(f)]. The gain below 0 dB even when the grid is disconnected (cases (d)(e)(f)) implies that the isolated DG and load system is stable, thus can be islanded. It is consistent with the time-domain simulation results in a later section that show, without any compensator, the islanding can be easily sustained.

The loop gains difference between grid-connected [(a)(b)(c)] and islanded [(d)(e)(f)] is due to the system structural change. One has a grid with relatively low impedance. The islanded system has no grid connected, or, equivalently, a grid with infinite impedance.

After being compensated, both the active power and reactive power loop gains are reshaped (the bottom two figures in Figure 12). The compensator design should be such that, the grid-connected loop gains [cases (a)(b)(c)] are below 0dB in order to keep the system stable, while the islanded loop gains [cases (d)(e)(f)] are above 0dB in order for effective AI detection. For the purpose of illustration, the peak value of the open loop gain is denoted as $G_p$, and the corresponding frequency is called $F_p$. Basically $G_p$ and $F_p$ together determine the dynamic characteristics of the AI control. From the design point of view, the larger $F_p$ and $G_p$, the stronger dynamics of the islanded system. However, there are some fundamental limits on the maxima of $G_p$ and $F_p$. For the active power AI scheme [Figure 12 (i) bottom figure], the limit on $F_p$ is due to the inertia of the DG. In this design, $F_p$ under the grid-disconnected condition is about 0.3Hz. This small $F_p$ indicates the slow response of the active power AI scheme to the loss of the

grid. In order to overcome the slow response due to small $F_p$, a high gain $G_p$ is necessary so that the frequency can be effectively driven out of the normal range for a given time. However, a high gain may potentially cause the DG instability, which sets the upper bound of the loop gain.

From the Bode plot shown in Figure 12 (ii) bottom figure, it can be seen that the $F_p$ of the reactive power AI loop gain is around 2.5Hz. In this case, the gain $G_p$ can be lower than the gain for the active power loop gain. This indicates that the reactive power AI scheme can respond faster than the active power AI scheme.

Another observation is that, once the rotating-machine-based DG is islanded, the difference in the loop gain due to the different power levels is insignificant while the previous study has shown that the loop gain of an inverter-based DG is very sensitive to the load power level [16].

### 3.4.2 Quality Factor

The loop gains with the different quality factors, $Q_f$ =0.0 and $Q_f$ =1.8, are compared with each other in Figure 13. The quality factor of a RLC load is defined as the ratio of the reactive power stored in the load inductor or capacitor to real power consumed by the resistor. For a load with fixed active power, the different quality factors imply varying the reactive power of the load, i.e. inductance and capacitance. Usually, a load with the quality factor of 1.8 is considered an extreme case for the islanding study. From Figure 13, it can be seen that the loop gains vary little with different quality factors for both grid-connected ((a)(b)) and islanded ((c)(d)) conditions. This is again quite different from the case in the inverter-based DG. The fundamental reason is the inertia difference. Generally, $Q_f$ represents the load inertia. The machine-based DG has large inertia and dominates the overall DG/load system inertia. As a result, different Qf makes little difference in the system dynamics.

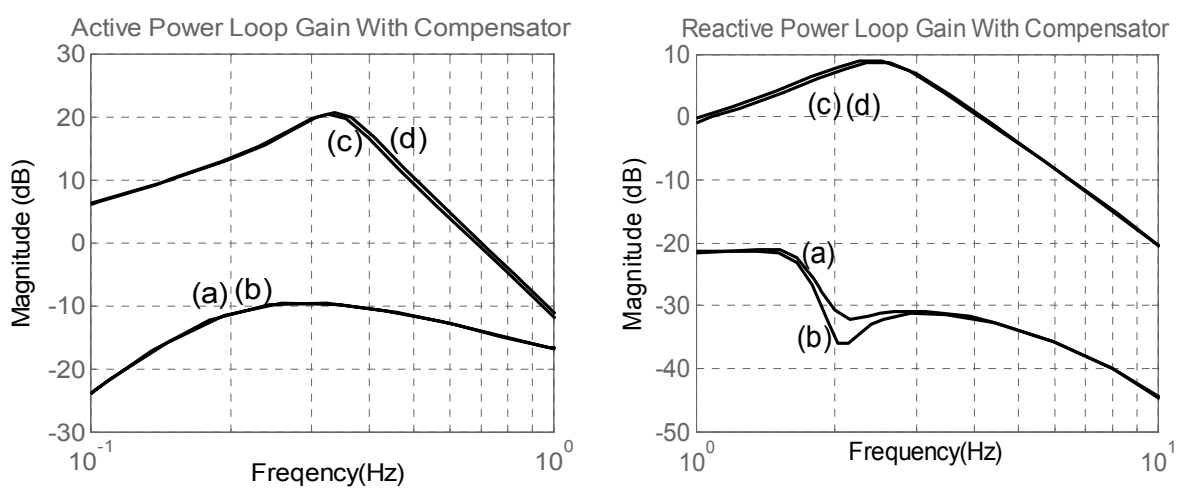


(i) Active power loops (ii) Reactive power loop gains

((a) (b) Grid-connected $Q_f$ =0.0 and $Q_f$ =1.8, (c)(d) Grid-disconnected $Q_f$ =0.0 and $Q_f$ =1.8)

Figure 13: Loop gains with different quality factors

### 3.4.3 Grid Impedance

The impact of the AI scheme on the grid stability is also investigated. With different grid impedance, especially high grid impedance (weak grid), the AI schemes may cause a stability issue (islanding is actually a special case with infinite grid impedance). Therefore, it is necessary to investigate its impact and specify its application limits.

The active and reactive power AI loop gains have been evaluated for the varying grid impedance from 5% to 40% (on the base of the DG power rating), as shown in Figure 14. It can be seen that the grid-connected active/reactive power AI loop gains [cases (a)(b)(c)] increase with the increasing grid impedance. When the grid impedance is approaching 40% (a rare but possible case), the system becomes marginally stable. Another observation is that the reactive power loop gains are more sensitive to the grid impedance than the active power loop gains.

As far as grid impedance is concerned, islanding is actually a special case that has infinite grid impedance. Between the infinite grid impedance (islanded) and finite grid impedance (grid-connected), the active AI controls always have certain design room by choosing appropriate gain so that their loop gains is separated by 0dB. The higher the grid impedance, however, will result in less design margins. Without sufficient margins, the system may risk instability.

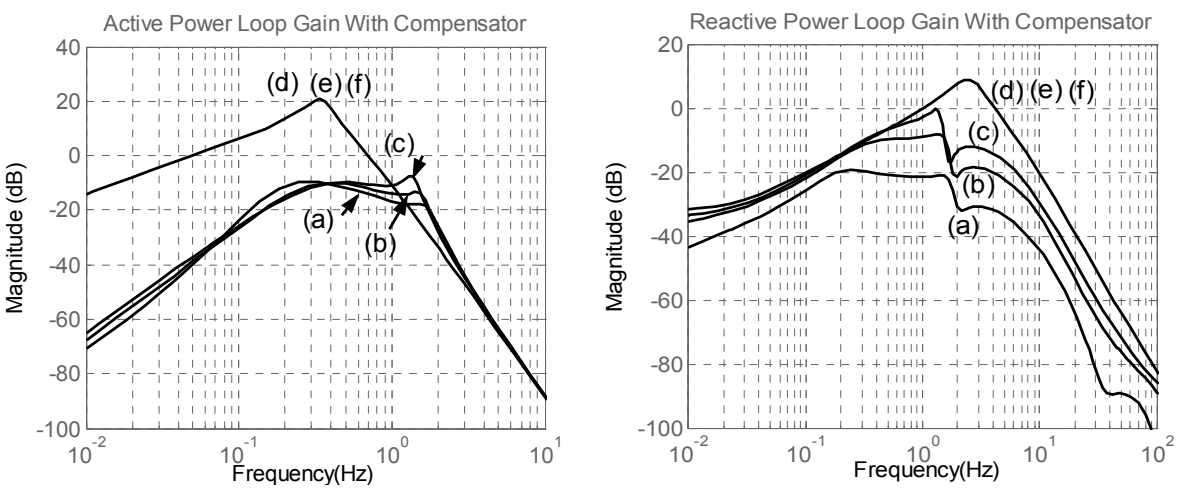


(i) Active power loop gains (ii) Reactive power loop gains

[(a) (b) (c) Grid-connected Xe=0.05 p.u.; Xe=0.2 p.u.; Xe=0.4 p.u. (d)(e)(f) Grid-disconnected Xe=0.05 p.u.; Xe=0.2 p.u.; Xe=0.4 p.u.]

Figure 14: Loop gains with different grid impedance

### 3.4.4 Motor Load

Induction motors constitute major part of the distribution load. Studies [15] show that the most important sensitivity influencing the system dynamics is the percentage of motors in a feeder. Variations in the motor inertia and impedances are not as great an influence on the system dynamics as the percentage of motors. The effects of the motor load on active/reactive power loop gains are evaluated when the load is composed of an induction motor (H=0.5MW/MVA, Power Rating=150kVA, comparable to the generator rating) and a capacitor for power factor correction.

Figure 15 shows the loop gains comparison between RLC load and motor load (with capacitor), both at unity power factor with the same power level. It can be seen that the active power loop gain of the induction motor load (Figure 15 (i) ((b)(d)) is lower than the loop gain with the RLC load (Figure 15 (i) ((a)(c)). It implies that the dynamics of the islanded system is slowed down by the induction motor load. In contrast, the reactive power AI scheme is still very effective with the motor load, shown in Fig. 3-7 (ii). It indicates that, the motor load is a worse case than RLC load for the active power scheme. For reactive power scheme, however, the motor load is easier to detect than RLC load.

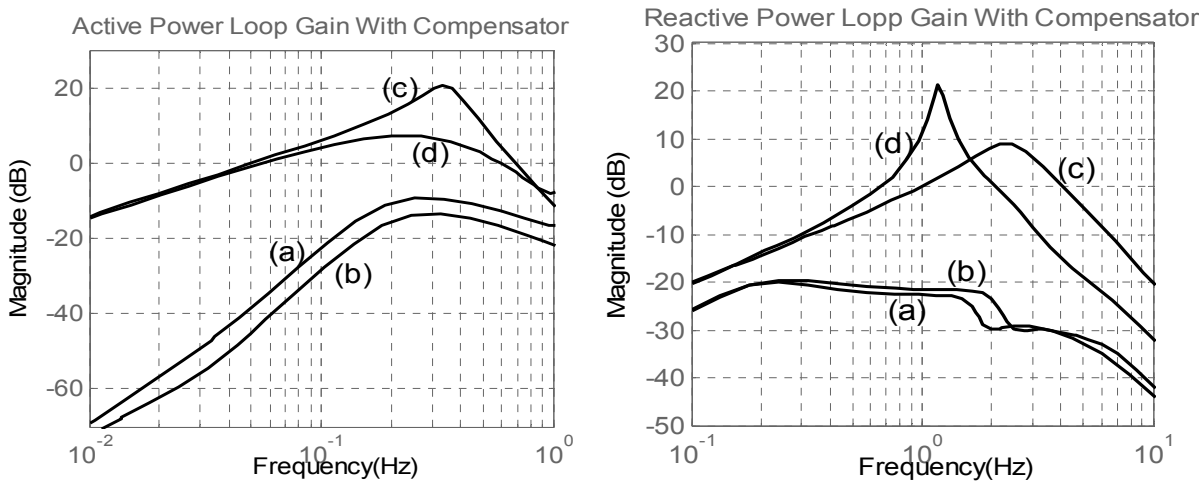


(i) Compensated active power loop gains (ii) Compensated reactive power loop gains

[(a) (c) Grid-connected/disconnected RLC load(P=0.54 p.u. and $Q_f$ =1.8) (b) (d) Grid-connected/disconnected motor load(P=0.54 p.u., Q=0.34 p.u. and C=600μF)]

Figure 15: Loop gains with RLC and motor load

### 3.4.5 Conclusions

In this chapter, we have investigated the dependence of the AI loop gains on various factors such as power output of the DG, quality factor, grid impedance, and motor loads. The effectiveness of both schemes is insensitive to power level and quality factor. The active power scheme is less effective with motor load than with RLC load, while the reactive power scheme is effective for both load conditions. When grid connected, the reactive power scheme is more sensitive to the grid impedance than the active power scheme. With the higher grid impedance, the stability margin of the reactive power scheme is reducing quicker than the active power scheme.

# 4. Performance Evaluation with Time-Domain Simulations

In the preceding chapter, the basic principles and design guidelines of the proposed two AI schemes have been discussed. In this section, time-domain simulations are carried out using PSCAD to validate the proposed schemes and to evaluate their effectiveness. The parameters of the DG and the load used in the simulations are given in the Appendix. The system used in the simulation consists of the grid, the synchronous generator, and the RLC or motor loads. A constant voltage source behind impedance is used to represent the grid. The local load and the DG are closely balanced. The loss of the grid is due to the trip of a utility breaker at steady state, and this is considered as the worst case for islanding detection.

The performance of the AI schemes is evaluated for both a static load and the induction machine load. For all islanding simulations, the grid is disconnected at t=1s.

## *4.1 Performance Evaluation With RLC Load*

### 4.1.1 Case 1: Baseline without AI Scheme

Before evaluating the performance of the proposed AI schemes, a baseline case without any AI schemes is simulated, shown in both Figure 16 and 17. The DG is operating at 88 kilowatts (kW), 60% of its rated power. The RLC load is 88 kW with quality factor Qf=1.8. Since the load and the DG are closely matched, the island can be sustained after the loss of the grid, because the variation in the frequency and the terminal voltage is so small that any passive scheme may not detect the islanding.

### 4.1.2 Case 2: Active Power Scheme with $Q_f$=1.8

The same DG output and load conditions, but with the active power AI scheme enabled, have been simulated. The simulation results are shown in Figure 16 (case 2). After the grid disconnection at t=1s, the frequency drifts quickly (within 2s) to go out of normal ranges (Figure 16(b)), while the voltage magnitude almost remains unchanged [Figure 16(a)]. Therefore, the active power AI scheme dominates the frequency dynamics, but has little effect on excitation (voltage) dynamics. Figure 16(c) shows the field voltage dynamics after islanding. Figure 16(d) shows the AI compensator output.

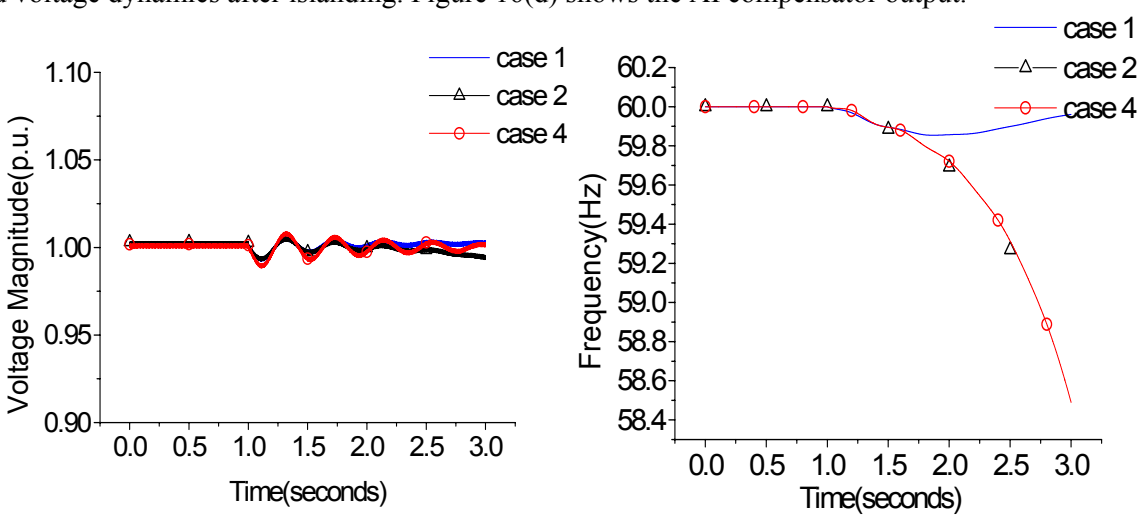


(a) Terminal voltage (b) Frequency

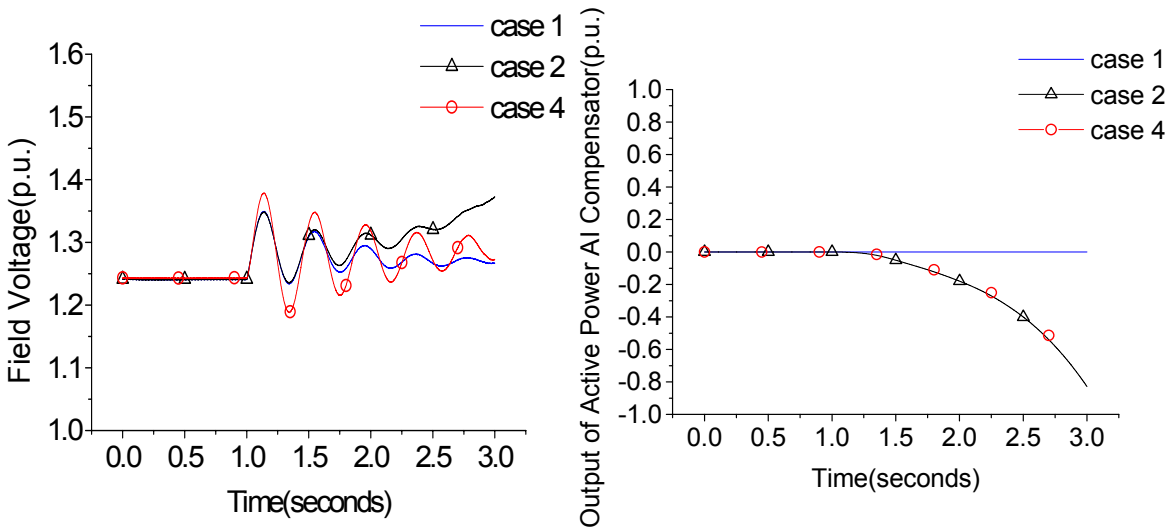


(c) Field voltage (d) AI compensator output

(Case 1: baseline without AI scheme P=88kW and $Q_f$=1.8; Case 2: active power AI scheme with P=88kW and $Q_f$=1.8; Case 4: active power AI scheme with P=88kW and $Q_f$=0.0)

Figure 16: Simulation results of the active power scheme in response to islanding at 1s

### 4.1.3 Case 3: Reactive Power Scheme with $Q_f$=1.8

Figure 17 shows that simulation results with the reactive power scheme is enabled. It can be seen that after islanding, the frequency [Figure 17(b) and the terminal voltage (Figure 17(a)] oscillate away quickly. The changes in frequency are caused by the fluctuating active power of the load when the terminal voltage is varying. In this case, the detection of the islanding can be triggered by either under/over frequency or an under/over voltage relay. Figure 17(c) shows the field voltage, which is saturated at 2 p.u., but the scheme is still effective.

### 4.1.4 Case 4: Active Power Scheme with $Q_f$=0.0

Figure 16 also shows the simulation results for a resistive load only ($Q_f$=0) (case 4) and with the active power AI scheme enabled. Compared with the simulation results for the load with $Q_f$=1.8 (case 2), the difference between the variations in the frequency and terminal voltage is negligible. This is well consistent with the analysis in the frequency domain.

### 4.1.5 Case 5: Reactive Power Scheme with $Q_f$=0.0

Figure 17 shows the simulation results for a resistive load only ($Q_f$=0) (case 5) , and with the reactive power AI scheme also enabled. Compared with the simulation results for the load of ($Q_f$=1.8) (case 3), the variations in the frequency [Figure 17(b)] and the terminal voltage[Figure 17(a)] 0 magnitude are only slightly different. It indicates that $Q_f$ has only a little impact on the reactive power AI scheme. This is also consistent with the analysis in the frequency domain.

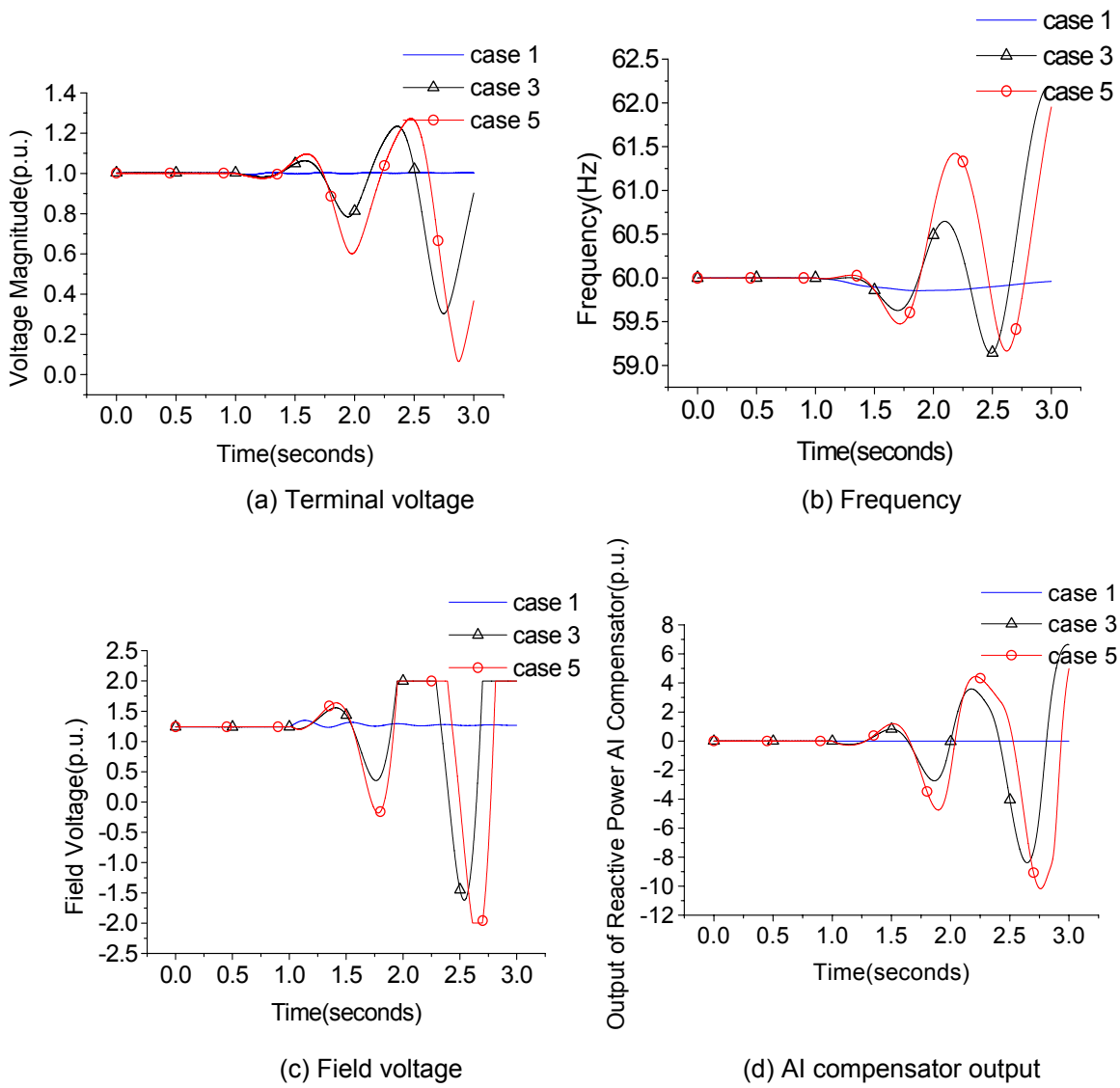


(Case 1: baseline without AI scheme P=88kW and $Q_f$=1.8; Case 3: reactive power AI scheme with P=88kW and $Q_f$=1.8; Case 5: reactive power AI scheme with P=88kW and $Q_f$=0.0)

Figure 17: Simulation results of the reactive power scheme in response to islanding at 1s

## *4.2 Performance Evaluation with Induction Motor Load*

As indicated in the previous section, motors form a major portion of system loads. Hence, it is important to investigate the motor load impact on the islanding protection. In this study, a generic induction motor is modeled to represent a general population of motors ranging in types from those in small residential/industrial applications to large motors. Studies [15] show that the most important sensitivity influencing the system dynamics is the percentage of motors at the load bus. Variations in the motor inertia and impedances are not as great an influence on the system dynamics as the percentage of motors. Here, the extreme case with 100% penetration of induction motor load (H=0.5MW/MVA, Power Rating=150 kVA) is simulated to evaluate its impact on the performance of the AI schemes. In the simulation, a capacitor is connected in parallel to the motor so as to compensate the reactive power of the induction motor.

### 4.2.1 Case 6: Baseline without AI Scheme and with Induction Motor Load

Before evaluating the performance of the proposed AI scheme for the induction motor load, a baseline case without any AI scheme is simulated, shown in Figure 18 (case 6). Since the power mismatch between the generator output and the motor load is very small, the initial oscillation of the islanded system is small and slow. However, the islanded system drastically changes its behavior after approximately 3 seconds of islanding. The voltage magnitude continues to drop so that the islanding cannot be sustained indefinitely.

Although the islanded system with the motor load seems to be unstable eventually, the detection of the islanding within 2 seconds is still difficult with the motor load due to its slow response in the first few seconds.

### 4.2.2 Case 7: Active Power AI Scheme with Induction Motor Load

The same conditions have been simulated except that the active power scheme is enabled and the simulation results are also shown in Figure 18 (case 7). Compared with the previous simulation results for RLC load, the active power AI scheme for the induction motor is not as effective as for the RLC load. In this case, actually, it fails to detect the islanding within a 2-second time window because the voltage and frequency are still within the normal ranges. This is consistent with the frequency-domain analysis.

### 4.2.3 Case 8: Reactive Power AI Scheme with Induction Motor Load

The same conditions have been simulated except that the reactive power scheme is enabled, and the simulation results are shown in Figure 18 (case 8). In this case, the voltage magnitude oscillates dramatically due to the reactive power AI scheme. The islanding can be easily detected by an over-voltage relay. The frequency also drifts away quickly. It concludes that the reactive power scheme is more effective for motor load than the active power scheme. The same conclusion is drawn in the frequency-domain analysis.

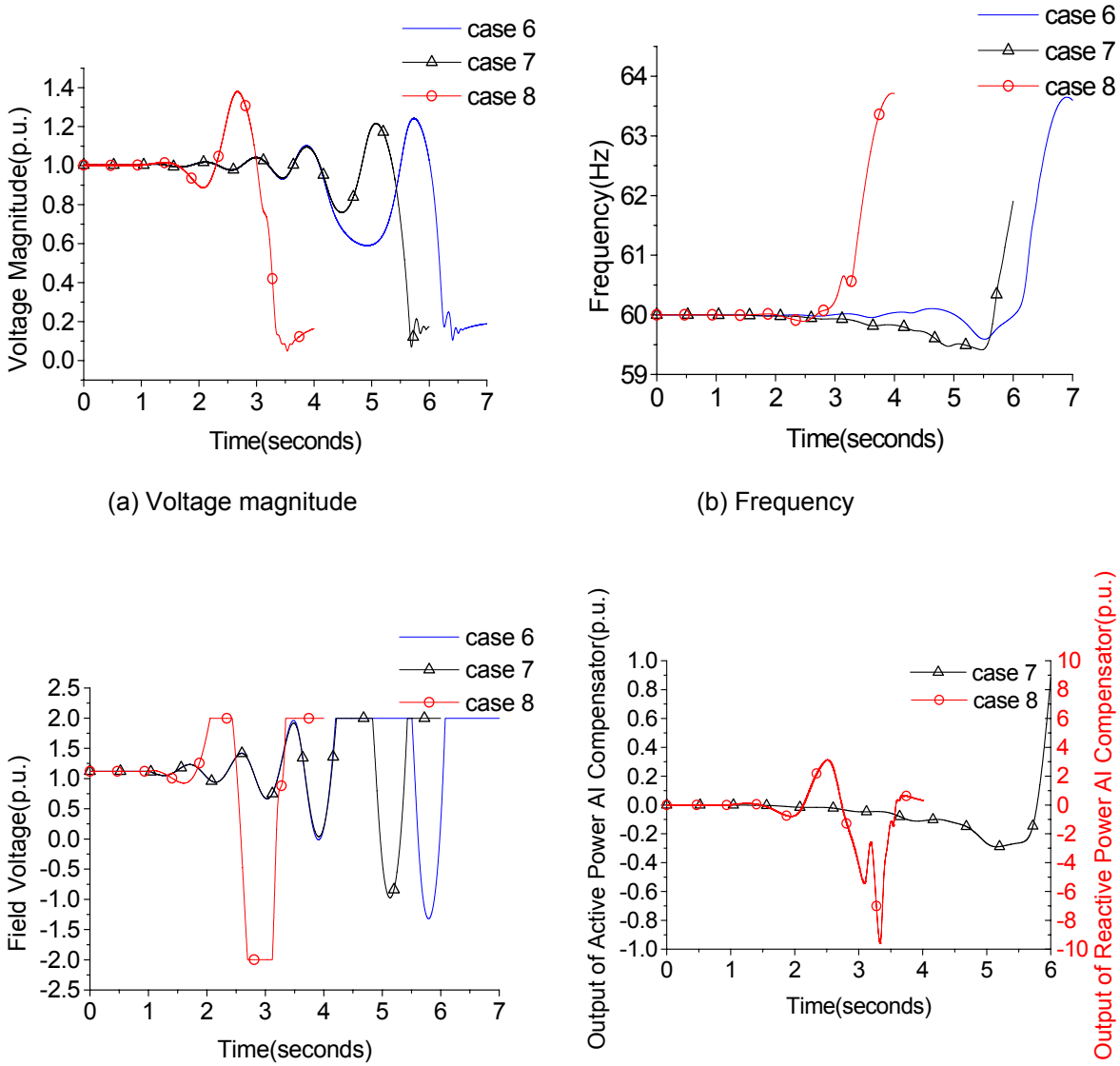


(a) Voltage magnitude

(b) Frequency

(c) Field voltage

(d) AI compensator output

(Case 6: baseline without any AI scheme for the Induction motor load; Case 7: active power AI scheme for the induction motor load; Case 8: reactive power AI scheme for the induction motor load)

Figure 18: Simulation results with the induction motor load in response to islanding at 1s

## *4.3 Performance Evaluation When the Grid Is Connected*

In the preceding section, the AI control performance of the active power and reactive power AI schemes have been demonstrated. Another major issue related to the performance of the AI schemes is the potential impact on the DG's normal operation under the grid-connected conditions. The following study will simulate a range of situations including oscillation in the grid frequency, a low voltage event and high grid impedance to investigate whether the proposed AI schemes have a significant impact or not.

### 4.3.1 Grid Disturbances

A robust AI scheme must distinguish between the actual loss of the grid and a grid disturbance with increasing penetration, distributed generation may become an integral part of the overall power generation system. Therefore, an unexpected tripping off line from the DG may cause severe impact on the system reliability and stability. One of those disturbances is a transient low voltage event. For some reasons (fault or start-up of large motors), the voltage could be lower than the normal ranges for an extended period of time. It's very difficult for any passive scheme to differentiate between the disturbance and the actual islanding.

In the following simulations, the active power and reactive power AI schemes are evaluated under a typical low-voltage ride through event. The performance is compared against the case without any AI scheme. A three-phase fault is applied at the high-voltage side of the distribution transformer at t=1s and lasts about 0.3 seconds. The responses of the frequency and voltage from the simulations are shown in Figure 19. It is demonstrated that the active power AI scheme is robust and resilient to this low voltage event. But the impact of the reactive power AI scheme has some negative effect, exaggerating the event when the DG is subjected to a low-voltage event. If widely deployed, this could compromise grid voltage stability following faults.

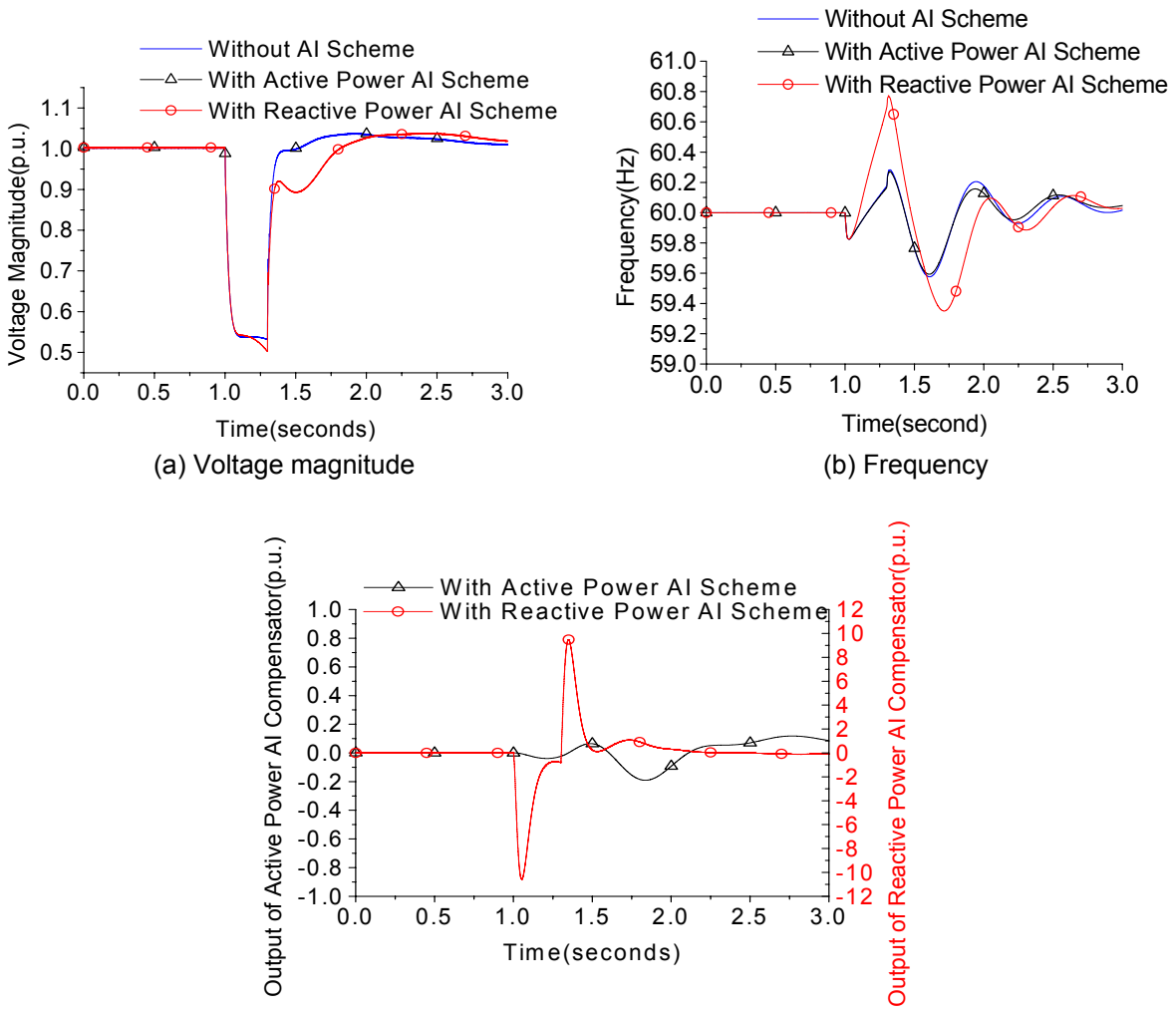


(a) Voltage magnitude

(b) Frequency

(c) AI compensator output

Figure 19: Simulation results of the generator response to a three-phase fault

### 4.3.2 Grid Impedances

There have been concerns over the stability impact caused by the positive feedback schemes, since the grid is not an ideal voltage source. Conceptually, if the gain of the positive feedback is too high or the grid is too weak, the DG may not operate stably due to the AI schemes. Therefore, there always has been the question of what are the stability bounds of the positive feedback schemes. Here the discussion only focuses on the strength of the grid. In the following simulation, the active power, and reactive power AI schemes are evaluated under extremely high grid impedance. The case with active power AI scheme has been simulated with a grid impedance Xe=0.5 p.u. (on the base of the DG power rating), and the AI scheme is enabled at t=1.0s. Here the grid is always connected even after 1s. As shown in Figure 20(a), the system is dynamically stable when the active power AI scheme is enabled. The case with reactive power AI scheme has been simulated with a grid impedance Xe=0.50 p.u. and the reactive power AI scheme is enabled at t=1.0s. As shown in Figure 20(b), the system is dynamically unstable when the

reactive power AI scheme is enabled. The high grid impedance causes the reactive power AI loop gain approaches 0dB, thus losing stability margins.

In order to maintain stability (especially transient stability, which imposes more margin requirement than small-signal stability), the design with sufficient margin is necessary. Therefore, for a given design, an upper bound of grid impedance must be specified as an application note, when applying the positive feedback AI schemes.

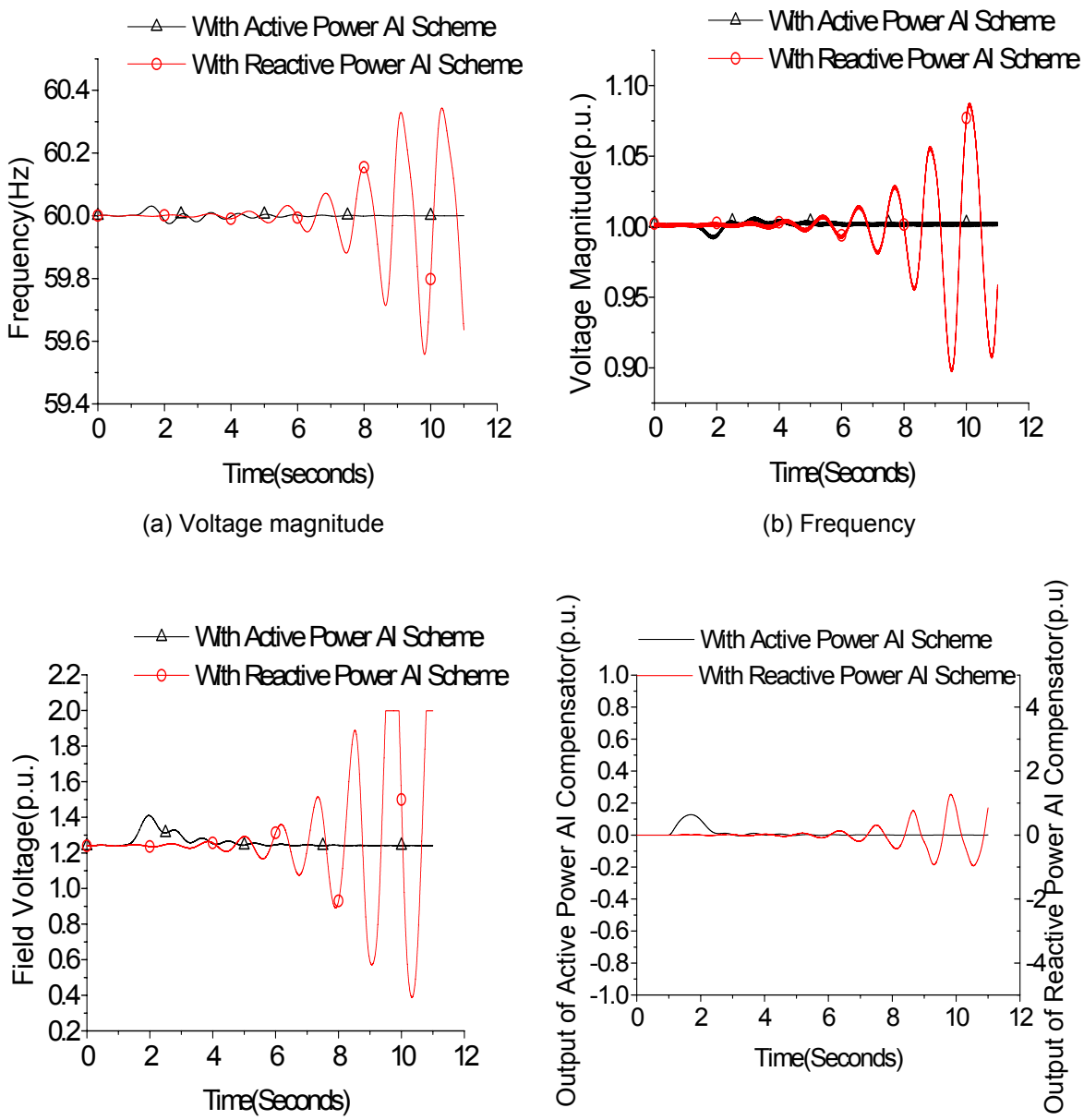


(a) Voltage magnitude

(b) Frequency

(c) Field voltage

(d) AI compensator output

Figure 20: Simulation results with high grid impedance

### 4.3.3 Grid Frequency Oscillations

Another disturbance event to test the performance of the new proposed schemes is a fluctuation in the grid frequency. This variation in the frequency may be attributed to some severe disturbances (faults or loss of a transmission line) occurring in the high-voltage level of the grid. Usually due to the large inertia of the power system, the rate of change of frequency is very low. One rare case simulated here is that the frequency oscillates between 59Hz and 61Hz at frequency of 1Hz. The simulation results with active/reactive power AI scheme enabled are shown in Figure 21. Even tested by so large variations in the frequency, there is little negative impact caused by the active/reactive power AI schemes.

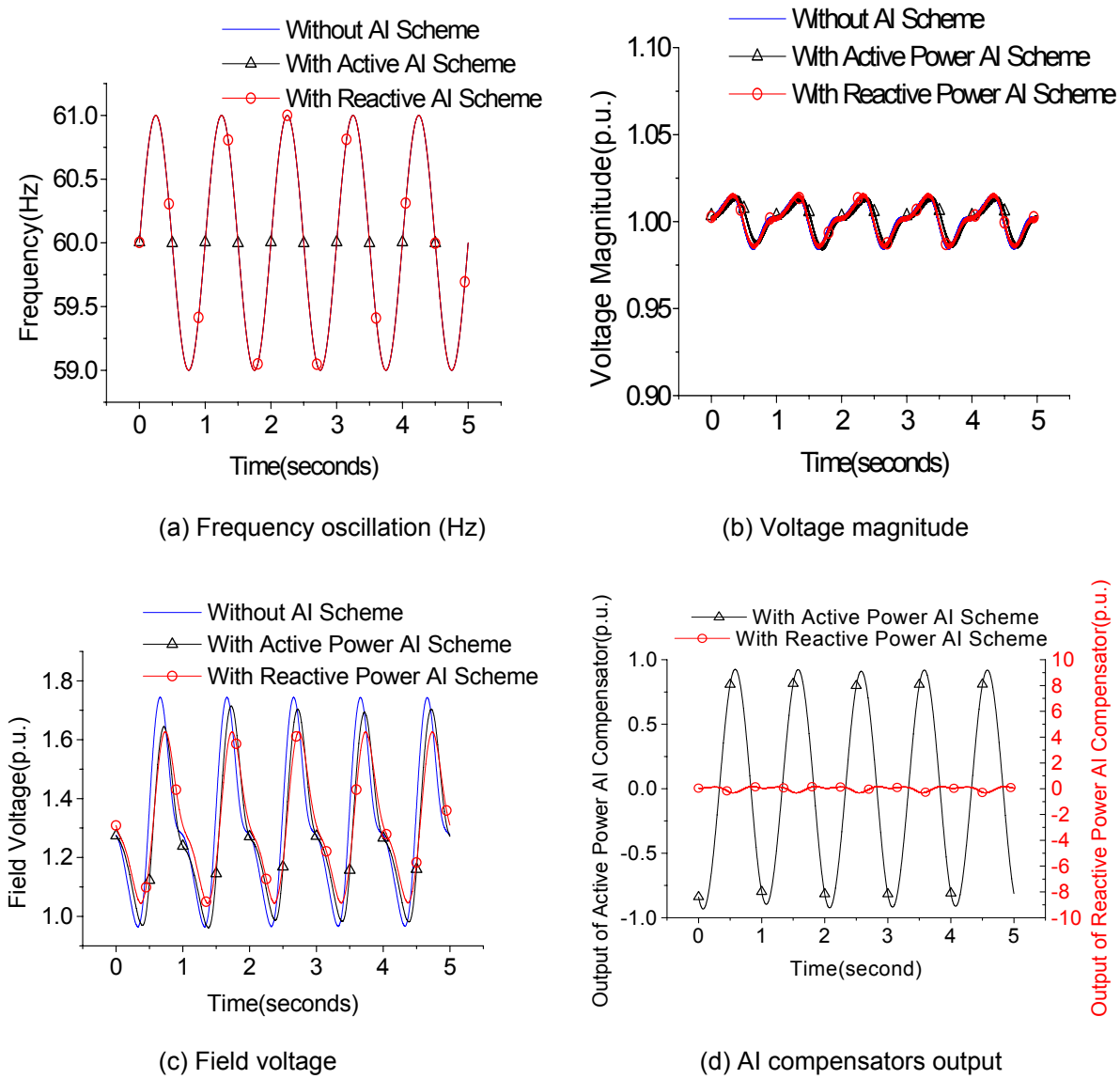


(a) Frequency oscillation (Hz)

(b) Voltage magnitude

(c) Field voltage

(d) AI compensators output

Figure 21: Simulation results of the generator response to the grid frequency oscillation

# Summary

## *5.1 Conclusions*

This report has proposed two new AI control schemes: namely the active power AI scheme and the reactive power AI scheme for synchronous machine-based distributed generations. These DGs include engine generators (diesel, natural gas, biomass, hydrogen) and gas turbines. In the report, the detailed discussions and simulation studies, including theoretical analysis and the design guidelines for the new AI schemes, have been covered.

The positive feedback created by the active/reactive power AI compensator will drive the frequency/voltage to be out of the normal ranges once the DG is islanded. One of the outstanding features is that the proposed schemes can show discrimination between actual islanding and other non-islanding disturbances. This is very hard for any passive scheme to achieve. Since the new schemes are designed as part of the DG control, the cost to implement the schemes is basically negligible.

In the first part of this report, the characteristics and modeling of the power system using Park's transformation was covered in considerable detail. After that, the positive feedback concept with the principles of the applications was introduced. With the frequency-domain analysis in MATLAB, the effectiveness of the new active/reactive power AI schemes have been evaluated over a wide range of load conditions. The preliminary study concludes that the reactive power AI scheme is more effective than the active power AI scheme. But the reactive power AI scheme is more likely to cause the DG to be unstable when the grid impedance is high (weak grid). The frequency-domain analysis conducted in MATLAB has been validated by the illustrative time-domain simulations conducted in PSCAD. The time-domain simulation also implies that the reactive power AI scheme has a slightly adverse effect when the DG is subjected to a low voltage event.

The preliminary study has discovered the following findings:

1. Without any active schemes, both the RLC load and induction motor load can be islanded for more than 2 seconds without being detected.

2. Both active power and reactive power AI schemes are very effective for RLC load, i.e., detecting islanding within 2.0s even when the power is closely matched between the generation and the load.

3. The impact of different power levels is very insignificant. That is, for a given scheme, it works at full power as well as at partial power.

4. The impact of different quality factor Qf is also insignificant. That is, for a given scheme, it works as effective with a high Qf load as with a low Qf load. This indicates that for synchronous machine-based DG AI testing, a resonant tank (RLC) load is not necessary.[1]

5. Substantial differences in performance were observed for the same AI scheme (e.g. active power AI scheme) with RLC load and induction motor load. Because induction motors form a large portion of actual loads, these results raise concern that passive load may not be adequate to evaluate the effectiveness of certain AI schemes.

[1] Latest IEEE P1547.1 testing standard draft is considering to use a simplified load other than RLC resonant tank for testing synchronous machine unintentional islanding protection function.

6. The reactive power AI scheme is superior to the active power AI scheme due to its high effectiveness for a high penetration of motor loads. However, the nominal operation of the DG equipped with the reactive power AI scheme can be affected more adversely by the grid impedance and voltage disturbances.

In summary, the new proposed AI schemes are highly reliable, robust to other non-islanding disturbances and easy for implementation.

## *5.2 Future Work*

In view of the progress described in the previous Chapters, the following directions are suggested as possible areas for further investigation:

1. **Optimum design of AI compensator**
This report has provided a systematic discussion on how to design the active/reactive power AI compensators with the assumption that such a compensator is linear. This is simple in the design but not optimum. The performance of the new proposed AI scheme could be improved if the AI compensator can adjust its gain to the variations of frequency or terminal voltage in real time. In doing so, the new AI schemes can be more effective and less sensitive to the grid impedance. This possibility can be explored in the further study.

2. **Multiple DG**
The discussion here is only limited to the situation with only one rotating machine DG present in the islanding. The proposed schemes, conceptually should work for the multiple DG but this has not been validated. Furthermore, the dynamical interaction between the inverter-based DG and rotating machine DG is an important consideration for the design of AI schemes. Therefore, extending the concept of positive feedback to multiple DGs will be the major task of next step.

3. **Test load for AI characterization**
This report shows that the RLC load representation may not represent the worst case to test some AI scheme. Further research is needed to develop models, which are simultaneously realistic and achievable in a test laboratory environment.

# 6. Appendix

## *6.1 Synchronous Machine Data*

The data for the generator used in the simulation studies is obtained from [17].

Machine rating: 150 kW.

Machine rated voltage (line-to-line RMS): 480V.

Inertia Constant : H =2.00 MW/MVA

Machine Reactance values (in pu):

Xd=10.823 pu ; Xq=5.325 pu; X'd=0.863 pu; X''d= 0.258 pu; X''q=0.304 pu;

Time constant value (in pu):

T'd0=2.11s;  T"d0=0.0227s; T"q0=0.176s; Xl=0.0892 pu; Ra=0.22 pu.

***Load Parameters (100 % of Load):***

R=1.536 ohms

L=2.26354 [mH]

C=3.108295 [mF]

***For the system with voltage and frequency control***

*Exciter Data:*

$K_1$=0.0625 pu; $T_1$=100 pu;

$K_2$=33 pu; $K_2$=0.02 sec;

$K_3$=1.0 pu; $K_2$=0.0159 sec.

*Governor Data:*

$T_G$=1.0 sec;

$R_G$=5% pu.

## *6.2 Induction Motor Data*

The data for the induction motor used in the simulation studies is obtained from [15].

Stator winding resistance $R_a$= 0.0068 pu;

Stator leakage inductance $L_1$= 0.1 pu;

Magnetizing inductance $L_m$= 3.4 pu;

Synchronous inductance $L_s$= 3.5 pu;

Rotor resistance $R_2$=0.018 pu;

Rotor leakage inductance $L_2$=0.07 pu;

Inertia constant H=0.5 MW/MVA

Load model exponent D=2 pu;

# 7. References


[1] *IEEE Standard for Interconnecting Distributed Resources with electric power systems*, IEEE Std 1547-2003, 2003.

[2] Warin, J.W. "Loss of mains protection," in *ERA Conference on Circuit protection for industrial and commercial installations, 1990,ERA 90-0001,* pp. 4/3/1-12.

[3] Cooper, C.B. "Standby generation, problems and prospective gains from parallel running," Keynote address, *International Power System Protection '89, Power System Conference, Singapore Polytechnic, Singapore, 1989.*

[4] Hopewell, P.D.; Jenkins, N.; Cross, A.D. "Loss-of-mains detection for small generators," *Electric Power Applications, IEE Proceedings-* , Volume: 143 Issue: 3 , pp. 225 –230, May 1996.

[5] Salman, S.K.; King, D.J. "Monitoring changes in system variables due to islanding condition and those due to disturbances at the utilities' network," in *Transmission and Distribution Conference, 1999 IEEE* , Volume: 2 , pp. 460 –465.

[6] Guillot, M.; Collombet, C.; Bertrand, P.; Gotzig, B. "Protection of embedded generation connected to a distribution network and loss of mains detection," in *Electricity Distribution, 2001. Part 1: Contributions. CIRED. 16th International Conference and Exhibition on (IEE Conf. Publ No. 482)*, Volume: vol. 4 , pp. 5.

[7] Redfern, M.A.; Usta, O.; Fielding, G., "Protection against loss of utility grid supply for a dispersed storage and generation unit," *Power Delivery, IEEE Transactions on* , Volume: 8 Issue: 3 , pp. 948 –954, July 1993.

[8] Redfern, M.A.; Barrett, J.I.; Usta, O, "A new loss of grid protection based on power measurements," in *Developments in Power System Protection,1997., Sixth International Conference on (Conf. Publ. No. 434)* , pp. 91 –94.

[9] Fu-Sheng, P.; Shyh-Jier, H, "A detection algorithm for islanding-prevention of dispersed consumer-owned storage and generating units ," *Energy Conversion, IEEE Transaction on* , Volume: 16 Issue: 4 , pp.346 –351, Dec. 2001.

[10] Salman, S.K.; King, D.J.; Weller, G., "New loss of mains detection algorithm for embedded generation using rate of change of voltage and changes in power factors," in Developments in Power System Protect*ion, 2001, Seventh International Conference on (IEE)*, pp.82 –85.

[11] Salman, S.K. "Detection of embedded generator islanding condition using elliptical trajectory technique," in *Developments in Power System Protection, Sixth International Conference on (Conf. Publ. No. 434) , 1997,* pp.103 –106.

[12] Jang, S.-I.; Kim, K.-H. "An Islanding Detection Method for Distributed Generations Using Voltage Unbalance and Total Harmonic Distortion of Current", *Power Delivery, IEEE Transactions on* , Volume: 19 , Issue: 2 , April 2004, pp 745 – 752.

[13] Kundur, P. *Power System Stability and Control*, EPRI, McGraw-Hill Inc., New-York, 1996.

[14] *IEEE recommended practices for excitation System Models for Power System Stability Studies*, IEEE Std 421.5-1992, Aug. 1992.

[15] Pereira, L.; Kosterev, D.; Mackin, P.; Davies, D.; Undrill, J.; Zhu, W. "An interim dynamic induction motor model for stability studies in WSCC," *IEEE Transactions on Power Systems*, Vol.17, No. 4, pp.1108-1115, November 2002.

[16] Zhihong, Y., et al. "Study and development of anti-islanding control for grid-connected inverters", GE global research center, Niskayuna, NY, 2003, report submitted to National Renewable Energy Laboratory (NREL).

[17] Jadric, I.; Boroyevich, D.; Jadric, M. "Modeling and Control of a Synchronous Generator with an Active DC Load", *IEEE transactions on Power Electronics*, Vol. 15 No.2, ,pp.303 – 311, March 2000.

# REPORT DOCUMENTATION PAGE

*Form Approved*
*OMB No. 0704-0188*

The public reporting burden for this collection of information is estimated to average 1 hour per response, including the time for reviewing instructions, searching existing data sources, gathering and maintaining the data needed, and completing and reviewing the collection of information. Send comments regarding this burden estimate or any other aspect of this collection of information, including suggestions for reducing the burden, to Department of Defense, Executive Services and Communications Directorate (0704-0188). Respondents should be aware that notwithstanding any other provision of law, no person shall be subject to any penalty for failing to comply with a collection of information if it does not display a currently valid OMB control number.
**PLEASE DO NOT RETURN YOUR FORM TO THE ABOVE ORGANIZATION.**

**1. REPORT DATE** *(DD-MM-YYYY)*
March 2006

**2. REPORT TYPE**
Subcontractor Report

**3. DATES COVERED** *(From - To)*
November 2001 - March 2004

**4. TITLE AND SUBTITLE**
Study and Development of Anti-Islanding Control for Synchronous Machine-Based Distributed Generators

**5a. CONTRACT NUMBER**
DE-AC36-99-GO10337

**5b. GRANT NUMBER**

**5c. PROGRAM ELEMENT NUMBER**

**6. AUTHOR(S)**
Z. Ye

**5d. PROJECT NUMBER**
NREL/SR-560-38018

**5e. TASK NUMBER**
DP05.1001

**5f. WORK UNIT NUMBER**

**7. PERFORMING ORGANIZATION NAME(S) AND ADDRESS(ES)**
GE Global Research Center
One Research Circle
Niskayuna, NY 12309

**8. PERFORMING ORGANIZATION REPORT NUMBER**
NAD-1-30605-01

**9. SPONSORING/MONITORING AGENCY NAME(S) AND ADDRESS(ES)**
National Renewable Energy Laboratory
1617 Cole Blvd.
Golden, CO 80401-3393

**10. SPONSOR/MONITOR'S ACRONYM(S)**
NREL

**11. SPONSORING/MONITORING AGENCY REPORT NUMBER**
NREL/SR-560-38018

**12. DISTRIBUTION AVAILABILITY STATEMENT**
National Technical Information Service
U.S. Department of Commerce
5285 Port Royal Road
Springfield, VA 22161

**13. SUPPLEMENTARY NOTES**
NREL Technical Monitor: Ben Kroposki

**14. ABSTRACT** *(Maximum 200 Words)*
This report summarizes the study and development of new active anti-islanding (AI) control schemes for synchronous machine-based distributed generators (DGs). These DGs include engine generators (diesel, natural gas, biomass, hydrogen) and gas turbines. The accomplishments of the work include advancing new AI control schemes that exhibit substantial improvement on non-detection zone for a static load, without power quality degradation; providing design guidelines and evaluating the effectiveness of the new schemes under various load conditions; and validating the new anti-islanding control schemes with a time-domain simulation in PSCAD.

**15. SUBJECT TERMS**
anti-islanding; synchronous distributed generators; engine generators; gas turbines; motor loads; power system modeling

| 16. SECURITY CLASSIFICATION OF: | | | 17. LIMITATION OF ABSTRACT | 18. NUMBER OF PAGES | 19a. NAME OF RESPONSIBLE PERSON |
|---|---|---|---|---|---|
| a. REPORT | b. ABSTRACT | c. THIS PAGE | | | 19b. TELEPHONE NUMBER (*Include area code*) |
| Unclassified | Unclassified | Unclassified | UL | | |

**Standard Form 298** (Rev. 8/98)
Prescribed by ANSI Std. Z39.18

F1146-E(12/2004)